VYSOKÉ UČENÍ TECHNICKÉ V BRNĚ
FAKULTA CHEMICKÁ

studentská odborná konference

CHEMIE JE ŽIVOT

30—11— 2023

SBORNÍK PŘÍSPĚVKŮ

Vysoké učení technické v Brně
Fakulta chemická

teva

Studentská odborná konference
Chemie je život 2023

Sborník příspěvků

Vysoké učení technické v Brně

Fakulta chemická, 30. listopadu 2023

Sponzorem konference je společnost Teva Pharmaceuticals CR, s.r.o.

Studentská odborná konference *Chemie je život 2023*
Sborník příspěvků

Editor: Ing. Jan Pernica.

Obsah

Sekce studentů bakalářských a magisterských studijních programů

Sekce studentů doktorských studijních programů
Tématický okruh vědy o živé přírodě a environmentální vědy

Sekce studentů doktorských studijních programů
Tématický okruh materiálové vědy

Sekce studentů bakalářských a magisterských studijních programů

Odstraňování tenzidů z odpadních vod

Leona Bačovská
Martina Repková, Jan Vespalec

Vysoké Učení Technické v Brně,
Fakulta chemická,
Ústav chemie a technologie ochrany životního prostředí
Purkyňova 464/118, 612 00 Brno, Česká republika
Leona.Bacovska@vutbr.cz

1 Úvod

S rapidní urbanizací a rozvojem průmyslových odvětví, například farmaceutického, textilního, prádelenského a těžebního, roste množství odpadní vody, která obsahuje perzistentní a toxické organické sloučeniny. Tyto biologicky obtížně rozložitelné sloučeniny mohou vykazovat karcinogenní a toxické účinky, a mohou tak vést k vážnému poškození zdraví a životního prostředí. Proto se vyvíjejí technologie, které umožní efektivní čištění těchto odpadních vod a minimalizují tak jejich negativní dopad na životní prostředí. Mezi tyto technologie se řadí například pokročilé oxidační procesy (AOP), které se ukazují jako vhodné technologie pro odstranění organického znečištění. Využívají se především pro čištění odpadních vod. Výhodou je, že jsou schopné odstranit i látky, které konvenční mechanicko-biologická čistírna odpadních vod nedokáže účinně odstranit.

Tato práce se zabývá odpadní vodou z prádelen. Prádelenská odpadní voda obsahuje zejména velké množství tenzidů. Tenzidy jsou velmi perzistentní a ve vodě rozpustné kontaminanty. Jako modelový tenzid byl vybrán dodecylsíran sodný (SDS), neboť je používán nejčastěji v mnoha domácích i průmyslových detergentech, kosmetice a produktech osobní potřeby, jakou jsou například šampony nebo pěny na holení. Využití SDS se zvyšuje rok za rokem. Odhaduje se, že SDS dnes představuje okolo 40 % ze všech využívaných detergentů. Nebezpečnost SDS tkví v jeho akumulaci v životním prostředí a organismech. SDS se řadí mezi xenobiotika a pokud se dostane do povrchových vod, může způsobit vážné poškození vodních ekosystémů[1].

Odstraňování tenzidů z odpadních vod je složité hlavně proto, že vytváří pěnová lůžka v technologiích pro čištění odpadních vod. Konvenční metody na odstraňování tenzidů z odpadních vod zahrnují chemické a elektrochemické oxidace, membránové technologie, fotokatalytickou degradaci, adsorpci, koagulaci a různé biologické metody[2]. Všechny tyto metody mají své výhody i nevýhody, kdy obecně čištění těchto vod s vysokým obsahem tenzidů je složité při využití jakékoliv z těchto metod. A další velmi slibnou metodou jsou pokročilé oxidační procesy, které byly řešeny i v této práci[3].

2 Experimentální část

2.1 Provedení experimentu

Jako modelový aniontový tenzid byl vybrán dodecylsíran sodný, neboť je snadno dostupný a nachází se až v 95 % produktů osobní potřeby. Před provedením každého experimentu bylo sklo vymyto methanolem, aby se zamezilo případné kontaminaci. Experiment byl proveden v různých vodních matricích, a to: v destilované vodě a v prádelenské modelové vodě. Pro každou matrici byli použity tři reakční systémy, a to: UV/H_2O_2, UV/O_3, UV/H_2O_2/O_3. Všechny experimenty probíhali na poloprovozní AOP jednotce, která je zobrazena na obrázku 1.

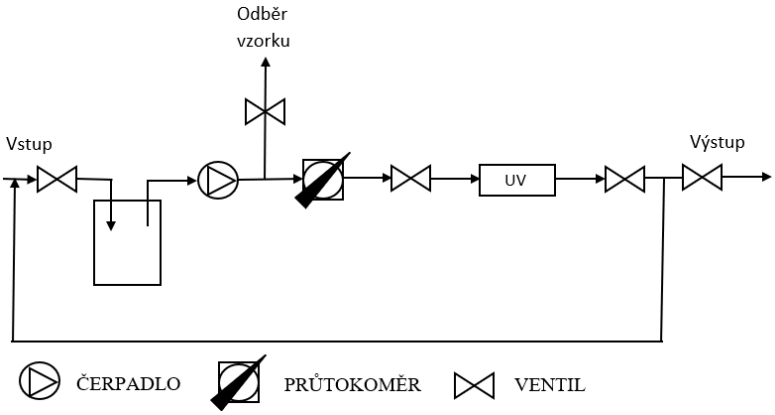

Obrázek 1 Schéma AOP jednotky

Experimenty probíhaly v cyklech. Každý experiment byl opakován minimálně 3x. Nastavení AOP jednotky bylo pro všechny experimenty stejné.

Tabulka 1 Nastavení AOP jednotky

Objem roztoku [l]	1
Počáteční koncentrace SDS [mg/l]	1,7
Průtok [l/min]	3

2.2 Stanovení SDS

Pro stanovení SDS byly použity kyvetové testy Spectroquant®. Aniontové tenzidy sulfonátového a síranového typu reagují s methylenovou modří a tvoří iontový pár, který je extrahován chloroformem. Modré zabarvení organické fáze je stanovováno fotometricky. Rozsah měření pro SDS je 0,05 – 2,12 mg/l.

2.3 Stanovení ozonu

Ozon byl stanovován kyvetovými testy Spectroquant®. Ozon reaguje v slabě okyseleném roztoku s dipropyl-p-fenylendiaminem a vytváří červeno-fialové barvivo, které se stanovuje fotometricky. Rozsah měření pro 10 mm kyvetu je 0,05 – 4 mg/l.

2.5 Stanovení peroxidu vodíku

Peroxid vodíku byl stanovován kolorimetrickou metodou. Jako titanové činidlo byl použit síran titanylu v kyselině sírové. Podstatou je reakce peroxidu vodíku s titaničitými ionty za vzniku kyseliny peroxotitaničité a žlutého zbarvení. Stanovení se provádí spektrofotometricky při vlnové délce 408 nm.

2.6 Degradace SDS v destilované vodě

Nejprve bylo zkoumáno použití samotného peroxidu, ozonu anebo UV. Do odměrné baňky o objemu 1 l bylo odváženo 1,7 mg SDS a doplněno destilovanou vodou. Následně bylo do baňky přidáno 700 µl peroxidu vodíku a baňka se dala do tmy. Po 15 minutách byla stanovena koncentrace SDS.

Destilovaná voda o objemu 1 l byla 15 minut ozonizována. Do této destilované vody bylo přidáno 1,7 mg SDS a baňka se uschovala do tmy. Po 15 minutách bylo stanoveno množství SDS a koncentrace ozonu.

Do odměrné baňky o objemu 1 l bylo přidáno 1,7 mg SDS a baňka se doplnila destilovanou vodou. Jednotka byla nastavena jako v parametrech výše a jednotka byla spuštěna. Po jednom cyklu byla stanovena koncentrace SDS.

2.6.1. Reakční systém UV/H_2O_2

Do odměrné baňky o objemu 1 l bylo odváženo 1,7 mg SDS. Baňka byla doplněna destilovanou vodou. Tento roztok byl přelit do kádinky. K tomuto roztoku bylo pipetováno 700 µl H_2O_2. Přístroj byl nastaven podle parametrů v *tabulce 4* a jednotka byla spuštěna. Provedl se vždy 1 cyklus. Po 1 cyklu byl odebrán vzorek a provedlo se stanovení SDS pomocí kyvetových testů a peroxidu vodíku pomocí UV-VIS spektrofotometru.

2.6.2. Reakční systém UV/O_3

Do kádinky byl napuštěn 1 l destilované vody a nechala se 15 minut ozonizovat. Po 15 minutách byl odebrán vzorek a pomocí kyvetových testů bylo stanoveno množství ozonu. Následně se do kádinky přidali 1,7 mg SDS a roztok byl promíchán. Přístroj byl nastaven stejně jako v případě systému UV/H_2O_2. Po 1 cyklu byl odebrán vzorek a provedlo se stanovení SDS a ozonu pomocí kyvetových testů a peroxidu vodíku pomocí UV-VIS spektrofotometru.

2.6.3. Reakční systém UV/H_2O_2/O_3

V případě reakčního systému UV/H_2O_2/O_3 se destilovaná voda nechala ozonizovat stejně jako u systému UV/O_3. Po ozonizaci se odebral vzorek a kyvetovými testy bylo stanoveno množství ozonu. Poté se přidali 1,7 mg SDS a 700 µl H_2O_2. Jednotka byla spuštěna a po jednom cyklu se odebral vzorek. Bylo stanoveno množství ozonu a SDS kyvetovými testy a množství peroxidu vodíku pomocí UV-VIS spektrofotometru.

2.7 Modelová voda

Experimenty probíhaly stejně jako v případě degradace SDS v destilované vodě.

2.7.1. Příprava prádelenské modelové vody

V odměrné baňce o objemu 1 l byly rozpuštěny chemikálie uvedené v tabulce 1.

Tabulka 2 Složení prádelenské modelové vody

Chemikálie	c [mg/l]
Bactopepton	25
Masový extrakt	20
Močovina	30
Chlorid vápenatý	140
Hydrogenfosforečnan didraselný	5
Síran hořečnatý	50
Síran amonný	5
SDS	1,7

3 Výsledky a diskuze

3.1 Experimenty v destilované vodě

Nejprve byly experimenty provedeny pouze v destilované vodě, aby se zjistilo, jak se SDS chová samostatně a jestli je degradovatelné pomocí AOP procesů. Počáteční koncentrace SDS byla 1,7 mg, tedy 5,89 μmol/l. U experimentů, kde byl použit peroxid vodíku, byla jeho počáteční koncentrace 6850 μmol/l.

Před degradací SDS systémy UV/H_2O_2, UV/O_3, UV/H_2O_2/O_3 bylo třeba vyzkoušet, jaký vliv na degradaci SDS má samotné působení UV, H_2O_2, anebo ozonu. Jak lze vidět na grafu 1 koncentrace SDS se při působení peroxidu a ozonu nesnížila prakticky vůbec. Při použití UV se snížila na 2,22 μmol/l o 62 %.

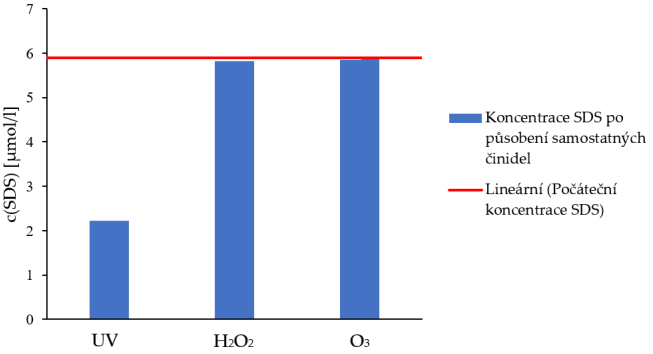

Graf 1 Vliv UV, H_2O_2 a O_3 na degradaci SDS

Při použití systému UV/H_2O_2 se koncentrace SDS po jednom cyklu snížila na 1,84 ± 0,11 µmol/l o 69 ± 1,9 % a koncentrace peroxidu vodíku na 1 490 ± 155 µmol/l o 78 ± 2,3 %. Jeden cyklus trval cca 18 vteřin a reakce tedy probíhá velmi rychle.

Dále byl na degradaci SDS použit systém UV/O_3. Koncentrace SDS po jednom cyklu vycházela na 1,88 ± 0,05 µmol/l v procentech snížení o 68 ± 0,9 %. Počáteční koncentrace O_3 byla 38,4 ± 9,6 µmol/l a po jednom cyklu byla koncentrace ozonu nulová. To znamená, že se tedy veškerý ozon rozložil. Velká odchylka u počáteční koncentrace ozonu vznikla pravděpodobně kvůli způsobu generování ozonu. Pokud molárně porovnáme systém UV/H_2O_2 a UV/O_3 zjistíme, že na degradaci 4 µmol SDS je potřeba 5360 µmol peroxidu vodíku a na degradaci téměř stejného množství SDS je potřeba jenom 38,4 µmol ozonu, což je o dost méně. Ozon se navíc spotřebuje všechen, a to může naznačovat nemalé provozní úspory v případě plného provozu.

Koncentrace SDS po degradaci v systému UV/H_2O_2/O_3 se snížila na 1,87 ± 0,13 µmol/l o 68 ± 2 % a peroxid vodíku na 1 957 ± 152 µmol/l o 71 ± 2,2 %. Počáteční koncentrace O_3 byla 26,3 ± 2,6 µmol/l a po jednom cyklu byla koncentrace stanovena na 8,54 ± 4,53 µmol/l. Toto je rozdíl oproti systému UV/O_3, kde byla konečná koncentrace ozonu nulová. V systému UV/H_2O_2/O_3 se ozonu spotřebuje méně než v systému UV/O_3 a všechen se nerozloží. To opět značí, že použití systému UV/O_3 by bylo provozně výhodnější.

V grafu 3 lze vidět srovnání jednotlivých systémů. Z hodnot vyplývá, že degradace SDS v destilované vodě je účinná všemi použitými systémy a míra účinnosti je srovnatelná u všech tří systémů. Limitujícím faktorem mohl být výkon UV lampy. Také proběhl pouze jeden cyklus a u systémů UV/H_2O_2 a UV/H_2O_2/O_3 byly po jednom cyklu naměřené poměrně velké reziduální koncentrace činidel. V budoucích experimentech by bylo proto zapotřebí provést cyklů více, aby se docílilo větší reziduální spotřeby činidel.

Na grafu 2 lze vidět srovnání jednotkových systémů. Z naměřených hodnot vyplývá, že na degradaci SDS jsou vhodné všechny použité systémy.

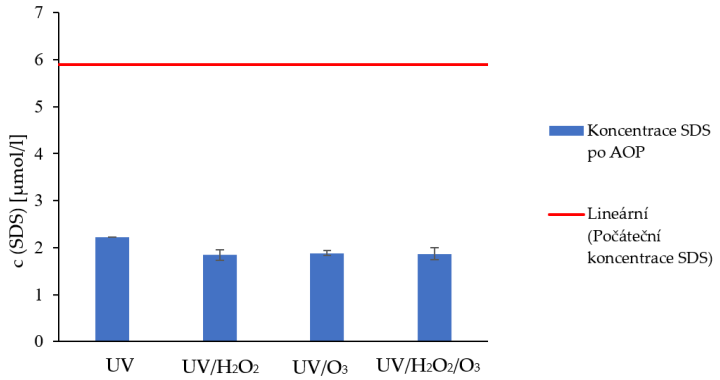

Graf 2 Degradace SDS v destilované vodě

3.2 Experimenty v prádelenské modelové vodě

Experimenty v prádelenské modelové vodě proběhly podobně jako v destilované vodě. V destilované vodě se ověřilo, že samotný ozon a peroxid vodíku nemají na degradaci SDS vliv, proto se v modelové vodě už tyto experimenty neprováděly. Po samotném UV se koncentrace SDS snížila na 3,1 µmol/l tedy o 47 %. To je méně jako v případě použití UV na SDS v destilované vodě. Důvodem mohlo být, že látky obsažené v prádelenské modelové vodě mohly absorbovat UV záření namísto SDS a tím zvyšovaly stabilitu SDS vůči tomuto záření.

Při použití systému UV/H_2O_2 se koncentrace SDS snížila na 2,65 ± 0,11 µmol/l o 55 ± 1,8 % a koncentrace peroxidu vodíku na 3 480 ± 200 µmol/l, snížení o 49 ± 3 %. V porovnání s destilovanou vodou, se peroxid vodíku spotřeboval pouze o 49 %, u destilované vody to bylo o 78 %. Mohlo to být způsobené tím, že látky obsažené v prádelenské odpadní vodě, mohli UV záření absorbovat a došlo tak ke kompetici o toto záření.

Koncentrace SDS se po procesu UV/O_3 snížila na 2,73 ± 0,11 µmol/l o 53 ± 1,9 %. Počáteční koncentrace ozonu byla 30,97 ± 3,37 µmol/l a po jednom cyklu 1,39 ± 0,12 µmol/l, snížení o 95 ± 0,4 % Hodnota ozonu vychází podobně jako v experimentech v destilované vodě a stejně jako tam, se i zde téměř všechen ozon spotřeboval. Lze tu pozorovat stejný trend jako v experimentech v destilované vodě. Na degradaci 2,8 µmol SDS, je potřeba 3 000 µmol/l peroxidu vodíku, ozonu je potřeba na degradaci stejného množství SDS pouze 30 µmol/l.

Při použití systému UV/H_2O_2/O_3 se koncentrace SDS snížila na 2,60 ± 0,14 µmol/l o 55 ± 2 % a koncentrace peroxidu vodíku na 3 370 ± 36 µmol/l, snížení o 51 ± 0,5 %. Počáteční koncentrace ozonu byla 29,51 ± 4,48 µmol/l a po jednom cyklu vycházela na 17,15 ± 2,02 µmol/l, snížení o 42 ± 7. Z výsledků vyplývá, že po systému UV/O_3 byla konečná koncentrace ozonu téměř nulová, kdežto v systému UV/H_2O_2/O_3 se nespotřebovala skoro ani polovina

Jak lze vidět na grafu 3 použití pokročilých oxidačních procesů na degradaci SDS v prádelenské modelové vodě je účinné všemi použitými systémy.

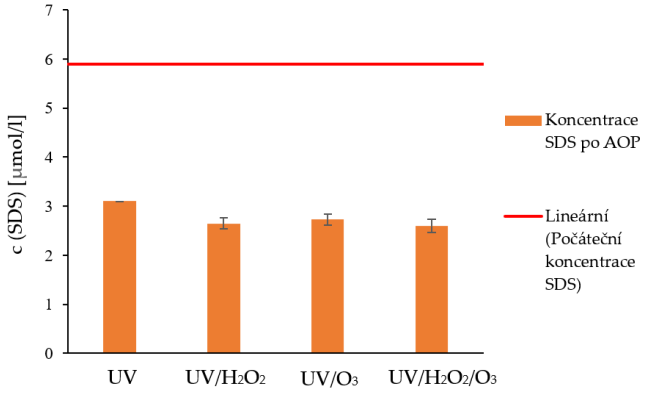

Graf 3 Degradace SDS v prádelenské modelové vodě

4 Závěr

Tato práce se zabývala odstraňováním tenzidů z odpadních vod. Na degradaci tenzidu SDS byly použity pokročilé oxidační procesy. Účinnost byla prokázána u všech použitých systémů v destilované i v prádelenské modelové vodě.

V destilované vodě po systému UV/H_2O_2 byla koncentrace SDS ponížena o 69 ± 1,9 % po UV/O_3 o 68 ± 0,9 % a po UV/H_2O_2/O_3 o 68 ± 2,0 %. Po samotném UV se koncentrace snížila o 62 %. V prádelenské modelové vodě hodnoty vyšly o něco vyšší než v případě destilované vody zhruba o 15 %. Po systému UV/H_2O_2 byla koncentrace SDS ponížena o 55 ± 1,8 %, po UV/O_3 o 53 ± 1,9 % a po UV/H_2O_2/O_3 o 55 ± 2,0 %. Po samotném UV se koncentrace SDS snížila o 47 %. Z naměřených hodnot vyplývá, že koncentrace SDS se v případě použití systémů UV/H_2O_2/O_3, UV/H_2O_2 a UV/O_3 sníží pouze nepatrně oproti použití samotného UV. Dále bylo zjištěno, že účinnost je téměř stejná pro všechny systémy, to mohlo být způsobeno podmínkami, které byly nastavené. Limitem mohl být výkon UV lampy. Také byl proveden pouze jeden cyklus a u systému UV/H_2O_2 a UV/H_2O_2/O_3 ještě zbývalo poměrně dost činidel, což mohlo být také limitujícím faktorem. Avšak ve všech případech byla účinnost degradace téměř stejná pro všechny tři systémy. Limitujícím faktorem mohlo být fakt, že se experiment prováděl pouze v jednom cyklu a u systému UV/H_2O_2 a UV/H_2O_2/O_3 zbývalo ještě poměrně dost činidel.

Pro detailnější pochopení mechanismu degradace tenzidů bude v dalším pokračování experimentu vyzkoušen i vliv dalších parametrů. Bude zkoumán vliv různé počáteční dávky peroxidu vodíku a ozonu, vliv pH a průtoku. Dále budou AOP použity na degradaci jiného tenzidu, než je SDS, a to konkrétně na dodecylbenzen sulfonát sodný. A také bude na degradaci použita ozonizace s využitím nanobublin.

5 Reference

1. BELÉN, Ana, Esteban GARCÍA, Kacper SZYMAŃSKI, Sylwia MOZIA a José ANTONIO SÁNCHEZ PÉREZ. Treatment of laundry wastewater by solar photo-Fenton process at pilot plant scale [online]. nedatováno. Dostupné z: doi:10.1007/s11356-020-11151-x/Published
2. ADAK, Asok, Manas BANDYOPADHYAY a Anjali PAL. Removal of anionic surfactant from wastewater by alumina: A case study. *Colloids and Surfaces A: Physicochemical and Engineering Aspects* [online]. 2005, **254**(1–3), 165–171. ISSN 09277757. Dostupné z: doi:10.1016/j.colsurfa.2004.12.004
3. MONDAL, Bijoli, Asok Adak 1∗ a Pallab DATTA. *UV-H 2 O 2 ADVANCED OXIDATION OF ANIONIC SURFACTANT: REACTION KINETICS, EFFECTS OF INTERFERING SUBSTANCES AND OPERATING CONDITIONS* [online]. 2019. Dostupné z: http://www.eemj.icpm.tuiasi.ro/;http://www.eemj.eu

Je lignín odpad, alebo obnoviteľný zdroj použiteľný v energetickom priemysle?

Matúš Majerčiak
Richard Nadányi, Aleš Ház

Slovenská technická univerzita v Bratislave,
Fakulta chemickej a potravinárskej technológie,
Ústav prírodných a syntetických polymérov, Oddelenie dreva, celulózy a papiera,
Radlinského 9, 812 37 Bratislava
xmajerciak@stuba.sk

1 Úvod do problematiky

V posledných rokoch sa čoraz viac zdôrazňuje potreba rýchlo znížiť, ak nie úplne obmedziť využitie fosílnych zdrojov vzhľadom na ich škodlivý vplyv na životné prostredie. Najživotaschopnejšie riešenie spočíva v používaní prírodných, obnoviteľných materiálov známych ako "obnoviteľné zdroje". Na rozdiel od fosílnych zdrojov tieto obnoviteľné zdroje ponúkajú udržateľné riešenie, pretože pochádzajú z prírody a sú obnoviteľné. Naopak, fosílne zdroje sú obmedzené a ich neustála spotreba neustále vyčerpáva obmedzené zásoby. Predpokladá sa, že tieto zásoby budú v priebehu niekoľkých desaťročí úplne vyčerpané, čo si vyžiada hľadanie alternatív, ktoré by ich mohli úplne nahradiť. Jedným z takýchto sľubných obnoviteľných zdrojov je biomasa, ktorá sa dostáva do popredia a nachádza široké uplatnenie v rôznych odvetviach, v ktorých sa tradične využívajú fosílne zdroje. Výhoda biomasy spočíva nielen v jej obnoviteľnosti, ale aj v jej bohatom energetickom obsahu. Významnou zložkou biomasy je lignocelulózová biomasa, ktorú tvorí suchá hmota rastlín zložená predovšetkým z celulózy, hemicelulózy a lignínu, usporiadaných v bunkovej stene do zložitých štruktúr. Lignín, vedľajší produkt celulózovo-papierenského priemyslu, má skrytý potenciál, ktorý možno využiť pri prechode na obnoviteľné zdroje. Ročná celosvetová produkcia lignínu v celulózo-papierenskom priemysle sa odhaduje na približne 70 x 10^6 ton, pričom väčšina sa rekuperuje ako nízkohodnotná energia [1]. Vzniká nový konsenzus, ktorý lignín nepovažuje za obyčajný odpad, ale za nezávislý, obnoviteľný zdroj, kde jeho spaľovanie by sa malo považovať za poslednú možnosť využitia [2]. V minulosti bol lignín často posudzovaný ako vedľajší produkt celulózového a papierenského priemyslu, ale nedávny výskum odhalil jeho potenciál ako cenného zdroja obnoviteľnej energie a chemikálií. Lignín sa dá rozložiť na menšie aromatické zlúčeniny a premeniť na rôzne vysokohodnotné chemikálie vrátane fenolov, vanilínu a BTX (benzén, toluén a xylén). Okrem toho biopalivá odvodené z lignínu, ako napríklad letecký benzín na báze lignínu, motorová nafta a benzín, vykazujú sľubné spaľovacie vlastnosti a kompatibilitu s existujúcimi systémami motorov a infraštruktúry. Ďalšou výhodou lignínu je, že vzniká ako vedľajší produkt pri spracovaní dreva na výrobu papiera a vyznačuje sa vysokým obsahom

energie. Skrytý potenciál lignínu a jeho energetický obsah sa môže využiť v rámci priemyslu, čo je v súlade s prevládajúcim posunom smerom k nahradeniu fosílnych zdrojov ako zdroja energie [3].

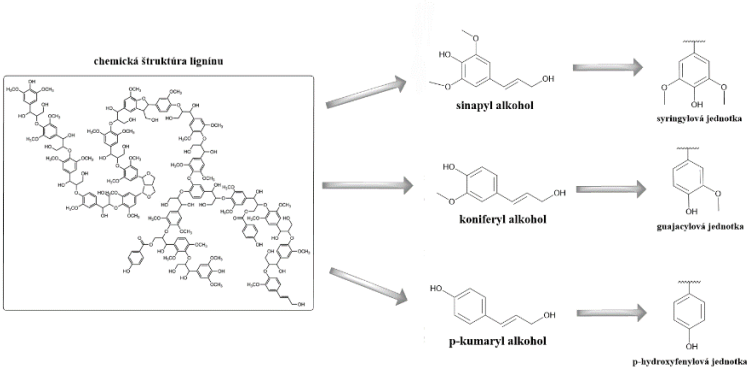

Obr. 1 *Podjednotky a štruktúra lignínu*

2 Experimentálna časť

Práca pojednáva o príprave lignínov, ktoré sa vyzrážali z rôznych zdrojov čiernych lúhov (**Tab. 1**). Čierny lúh (ČL) je vedľajší produkt sulfátového procesu, ktorý sa v celulózovo-papierenskom priemysle používa na premenu buničiny na papierovinu. Je to vodný roztok, ktorý obsahuje zvyšky lignínu, hemicelulózu a anorganické chemikálie.. V práci sa ďalej porovnávali finálne vlastnosti lignínov v závislosti od použitia rôznej koncentrácie kyseliny sírovej, ktorá sa použila pri zrážaní lignínov z ČL.

Z viacerých možností prípravy lignínu sa vybral postup, kedy sa pripravil požadovaný sulfátový lignín, ktorý pochádzal z čierneho výluhu Mondi SCP, Ružomberok. Vyrobený bol postupným okysľovaním čierneho lúhu pomocou CO_2. Pri procese zrážania lignínu sa sledoval vplyv podmienok (pH a teploty) na vlastnosti lignínu. Cieľom bola optimalizácia celkového procesu a podmienok – teplota, pH pri príprave lignínu. Aby sa zjednodušila komplexná náročnosť experimentu urobil sa plánovaný experiment. Výsledky z pripravených lignínov sa porovnali a ocharakterizovali pomocou analytických metód. Z optimalizácie procesu sa vybrali najvýhodnejšie parametre (pH a teplota) na prípravu finálneho lignínu (FL – lignín s najlepšími vlastnosťami). Finálny lignín sa modifikoval pomocou rôznych modifikátorov. Tu bolo cieľom využiť chemickú modifikáciu na úpravu lignínovej matrice a tým zlepšiť jeho konečné vlastnosti. Pripravené vzorky lignínov s vybranými modifikátormi sa porovnali na základe ich fyzikálnych a chemických vlastností. Následne sa vyhodnotila účinnosť modifikačných postupov na základe dostupných analytických metód UV-Vis, Kalorimetria (HHV), Termogravimetrická analýza (TGA) a FTIR analýza. Výsledné stanovenia sa porovnali a vybrali sa ligníny s najlepšími vlastnosťami, ktoré predstavujú vhodný základ obnoviteľného zdroja použiteľného v energetickom priemysle, alebo ako nahradzajúcu surovinu na výrobu syntetických polymérov, čo prispeje k hľadaniu trvalo udržateľných, obnoviteľných alternatívnych zdrojov.

2.1 Zrážanie lignínov z rôznych druhov čiernych lúhov

Čierny lúh (ČL) je vedľajším produktom procesov rozvlákňovania fytomasy a obsahuje veľké množstvo anorganických solí, taktiež polysacharidy a lignín. [4]. V práci sa sledoval vplyv izolácie lignínu z rôznych vstupných surovín čierneho lúhu, kde sa zmeny výsledných vlastností skúmali pomocou analytických metód, ako je kalorimetria, prvková analýza (C, H, N a S) a stanovenie obsahu anorganických látok (popola) [6].

Tab. 1 *Príprava lignínov z rôznych druhov ČL*

ČL	Varenie buničiny	Surovina ČL	Podmienky zrážania
ČL 1 pH 12,9 ± 0,3	Alkalická nátronová buničina	Jednoročné rastliny - OP Papiereň, s.r.o. (Olšany, CZ)	Bez riedenia ČL, teplota 53 °C ± 2 °C. Titrácia s rôznymi koncentráciami H_2SO_4 (5 %, 25 %, 50 % a 72 %) pri pH 5. Sušenie filtrátu do konštantnej hmotnosti (24 h, 25 °C) - prírastok suchého lignínu.
ČL 2 pH 12,9 ± 0,3	Alkalická nátronová buničina	Jednoročné rastliny - OP Papiereň, s.r.o. (Olšany, CZ)	Bez riedenia ČL, teplota 53 °C ± 2 °C. Titrácia 5% H_2SO_4 na pH 3. Sušenie filtrátu do konštantnej hmotnosti (24 h, 25 °C) - prírastok suchého lignínu.
ČL 3 pH 12.8 ± 0.4	Sulfátová buničina	Drevina - Bukóza Holding a.s. (SK)	Bez riedenia ČL, teplota 53 °C ± 2 °C. Titrácia 5% H_2SO_4 na pH 3. Sušenie filtrátu do konštantnej hmotnosti (24 h, 25 °C) - zisk suchého lignínu.
ČL 4 pH=13,75	Nátronová buničina (bez obsahu síry)	Jednoročné rastliny (konope)	1 až 2 l ČL sa okyslilo 50 % H_2SO_4 pri pH 3. Keď zmes dosiahla pH 3, doplnila sa po vrch kadičky demi vodou, po usadení (12 h) sa zrazenina dekantovala a prefiltrovala. Filtrát sa vysušil na vzduchu a vysušil v lyofilizátore (24 h).
ČL 5 pH = 9,5	Sulfátová bunčina	Ihličnaté a listnaté stromy	Sulfát ČL sa okyslil 50 % H_2SO_4 - zisk alkalického lignínu. Alkalický lignín sa zriedil vodou v pomere 1 : 8. Lignín sa okyslil pri teplote 55 °C na pH 3,5. Použil sa poloprevádzkovaný reaktor na zrážanie CO_2, kde sa premýval v dvoch membránach pri tlaku 2 bary - zisk dvoch filtračných koláčov. Tie sa stlačili pri tlaku 350 barov. Následne sa pokračovalo v praní vodou pri teplote 60 °C a tlaku 2 bary. Po premytí sa koláče lignínu opäť vytlačili pri tlaku 350 barov. Filtrát sa vysušil v lyofilizátore (24 h).
ČL 6	Alkalická nátronová buničiana	Jednoročné rastliny – OP Papiereň,	H_2SO_4 zriedená demineralizovanou vodou v hmotnostnom pomere 1 : 1 sa pridalo do ČL do hodnoty pH 3.. Filtrát sa

		s.r.o. (Olšany, CZ)	niekoľkokrát premyl horúcou vodou. V poslednom kroku sa lignín vysušil na lyofilizátore (24 h, 25 °C).

2.2 Plánovaný experiment – príprava finálneho lignínu

Pri hľadaní najvhodnejšieho lignínu, ktorý by sa pripravil pri určitých podmienkach – teplota a pH, sa použil plánovaný experiment. Pre náš experiment sa vybral 5-úrovňový 2-faktorový experiment. Sledovaná závislosť podliehala dvom faktorom: teplote a hodnote pH. Hodnotiace parameter boli: hmotnosť výťažkov, podmienky prípravy a kvalita pripraveného produktu. Vzorky sa pripravili zrážaním alkali- lignínu s kyselinou sírovou pri rôznych podmienkach. Menila sa hodnota pH a teplota, pri ktorej sa lignín pripravoval (***Tab. 3***).

Tab. 2 *Jednotlivé pokusy plánovaného experimentu*

Faktor (k)	Jadro plánu (NC)	Hviezdne body (NS)	Nulové body (N0)	Alfa (α)	Všetky pokusy (N)
2	4	4	5	1,414	13

Podľa literárnej rešerše a orientačných experimentov sa stanovil rozsah zvolených faktorov pre plánovaný experiment. Výpočty konečných hodnôt boli prepočítané z kódovaných hodnôt a následne získané pomocou programu exper implementovaného v MS Excel.

Tab. 3 *Kódované (matematické) a reálne hodnoty pre 5-úrovňový 2-faktorový experiment*

Faktor	-alfa(-α)	-1	0	1	alfa (α)	Yi
Teplota[°C]	25,0	33,1	52,5	72,0	80,0	19,4
pH	2,0	2,4	3,25	4,1	4,5	0,9

	Matematické hodnoty		Reálne hodnoty	
Vzorka	Teplota	pH	Teplota [°C]	pH
1	-1	-1	33,05	2,37
2	1	-1	71,95	2,37
3	-1	1	33,05	4,13
4	1	1	71,95	4,13
5	-1,414	0	25	3,25
6	1,414	0	80	3,25
7	0	-1,414	52,5	2,00
8	0	1,414	52,5	4,5
9	0	0	52,5	3,25

10	0	0	52,5	3,25
11	0	0	52,5	3,25
12	0	0	52,5	3,25
13	0	0	52,5	3,25

Optimalizácie podmienok prípravy finálneho lignínu (FL) boli vypočítané pomocou doplnku Riešiteľ v MS Excel.

2.3 Príprava finálneho lignínu

Lignín sa pripravil rozpustením alkalického lignínu s vodou v kadičke s pomerom 1:8 (alkalický lignín : voda). Suspenzia sa za stáleho miešania okysľovala 50 % kyselinou sírovou. Po dosiahnutí pH 2 sa reakčná zmes začala zahrievať. Keď suspenzia dosiahla 80 °C, nechala sa miešať 1 hodinu. Potom sa suspenzia prefiltrovala cez Büchnerov lievik. Filtračný koláč sa premyl horúcou vodou, aby sa zneutralizovala zvyšková kyselina (schéma na ***Obr. 2***).

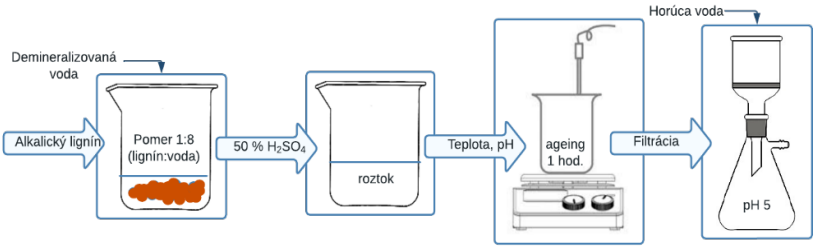

Obr. 2 *Schéma zrážania finálneho lignínu*

2.4 Modifikácia finálneho lignínu - zeleným modifikátorom

Finálny lignín sa modifikoval tzv. zeleným modifikátorom (ľahko degradovateľný – šetrný k prírode). Prvá modifikácia sa robila pomocou glycerínu, kde sa očakávala interakcia s matricou lignínu. Pri modifikáciách sa používal práškový lignín (FL) rozpustený v požadovanom množstve vody, aby sa zachoval pomer 1:8 (lignín : voda). Prvá modifikácia zahŕňala prípravu lignínu s 5, 10, 15, 20, 25, 30 % prídavkom glycerínu. Na modifikáciu sa použilo 10 g vstupného lignínu, ktorý sa zmiešal s 80 ml vody a zahrial na teplotu 60 °C. Vzniknutá suspenzia sa miešala 30 minút, čo bol čas potrebný na modifikáciu. Pomer vody a lignínu sa zachoval 1:8 (lignín : voda). Vzniknuté suspenzie modifikovaných lignínov sa prefiltrovali cez Büchnerov lievik pomocou vodnej vývevy. Vzniknuté filtračné koláče sa premyli 100 ml demineralizovanou vodou. Následne sa nechali vysušiť v lyofilizátore, aby sa stali absolútne suchými. Na záver sa pripravil referenčný preparát, ktorý pozostával z finálneho lignínu (MOD) pri podmienkach modifikácie (teplota 60 °C), ale bez prídavku modifikátora. Finálne vlastnosti sa ocharakterizovali pomocou

analytických metód ako: UV-Vis, kalorimetria (HHV), stanovenie anorganických látok (popol), termogravimetrická analýza (TGA).

2.5 Modifikácia finálneho lignínu – rôzne modifikátory

Vzorky lignínov sa pripravili pomocou modifikácie finálneho lignínu (FL). Celkovo bolo pripravených 17 vzoriek modifikovaných lignínov, ktoré sa odlišovali podmienkami prípravy, ako aj typom modifikácie. Na modifikáciu lignínu sa použili rôzne modifikátory za rôznych podmienok modifikácie (teplota a čas), ako aj v rôznych koncentráciách s cieľom pridania nových funkčných skupín – acetylová (ACL), acetálová (DMPL), ale aj esterová (SESAL, SEANL,). Na modifikáciu sa použili rôzne činidlá, niektoré aj v kombinácii so smrekovým extraktom, alebo vedľajším produktom po lisovaní slnečnicového oleja. Následne sa modifikované ligníny vysušili do konštantnej hmotnosti a ocharakterizovali pomocou analytických metód ako UV-Vis, FTIR analýza a Termogravimetrická analýza (TGA).

3 Výsledky a diskusia

3.1 Vplyv kyseliny sírovej na konečné vlastnosti vyzrážaných lignínov

Z *Tab. 4* vyplýva, že koncentrácia kyseliny sírovej mierne ovplyvňuje výťažok, ale len pri použití 5 % kyseliny sírovej, kde je výťažok 18,3 %. Najväčší výťažok (20,6%) sa dosiahol pri zrážaní za pomoci 72 % kyseliny sírovej. Z výsledkov vyplýva, že koncentrácia kyseliny nemá zásadný vplyv na výťažok lignínu (vlastnosti ovplyvňujú hlavne podmienky pri zrážaní). Obsah popola je nízky a pohybuje sa v rozmedzí od 0,66 do 0,97 %. Hodnota spalného tepla je takmer rovnaká pre všetky štyri vzorky. Táto hodnota nie je ovplyvnená použitou kyselinou v rôznych koncentráciách. Namerané hodnoty sa pohybovali od 26,20 do 26,86 MJ/kg.

Tab. 4 *Výťažky vyzrážaného lignínu pri použití kyseliny sírovej s rôznymi koncentráciami (5, 25, 50, 72 %), % popola a hodnoty spalného tepla (HHV)*

Koncentrácia (%)	Výťažok (% a.s.)	Popol (%)	Hodnota spalného tepla (HHV) (MJ/kg)
5	18,29	0,97	26,29
25	20,03	0,66	26,20
50	20,18	0,72	26,69
72	20,57	0,85	26,86

Percentuálne zastúpenie prvkov C, H, N, O a S zo zrážaných lignínov je uvedené v ***Tab. 5.*** Pomery atómov O/C izolovaného lignínu sú približne v rozmedzí od 0,29 do 0,33 a pomery atómov H/C sú v rozmedzí 1,18 - 1,23. Zastúpenie prvkov v priemerných hmotnostných percentách pre štyri vzorky je nasledovné: C 64,78 ± 0,87 %, H 6,44 ± 0,09 %, N 1,13 ± 0,03 %, S 0,06 ± 0,01 % a O 26,79 ± 0,95 %. Z výsledkov opäť vyplýva, že použitie kyseliny sírovej s rôznymi koncentráciami na vyzrážanie lignínu z čierneho lúhu nemá významný vplyv na prvkové zloženie študovaných lignínov. Relatívne nízky obsah síry v

procese zrážania umožňuje použiť tieto ligníny ako suroviny na výrobu výrobkov s pridanou hodnotou.

Tab. 5 *Elementárna analýza prvkov a atómové pomery H/C, O/C*

Rôzna koncentrácia H_2SO_4 (%)	Elementárna analýza (%)					H/C	O/C
	N	C	H	S	O		
5	1,11	65,75	6,46	0,06	25,59	1,18	0,29
25	1,12	63,64	6,54	0,07	26,95	1,23	0,33
50	1,12	64,84	6,33	0,04	27,96	1,17	0,31
75	1,18	64,90	6,42	0,07	25,66	1,19	0,31

3.2 Charakterizácia lignínov pripravených zrážaním s kyselinou sírovou

Na charakterizáciu komerčných lignosulfonátov sa použili tieto metódy: elementárna analýza, stanovenie popola a stanovenie spalného tepla. V ***Tab. 6*** sú zhrnuté výsledné hodnoty získané z analytických metód. V prípade komerčných lignosulfonátov sa obsah uhlíka stanovený elementárnou analýzou pohyboval od 42,9 % (DP – 02) do 52,5 % (Vanisperse CB), obsah dusíka bol od 0,09 % do 0,16 %, obsah vodíka od 4,08 % do 5,35 % a obsah síry od 2,96 % (Vanisperse CB) do 7,15 % (DP – 03). Obsah popola v týchto vzorkách sa pohyboval od 10,8 % (Orzan S) do 34,2 % (Vanisperse CB). Výhrevnosť lignosulfonátov sa pohybovala od 17,3 (DP – 02) do 20,61 (Vanisperse CB) MJ/kg.

Spomedzi všetkých vzoriek mal lignín L-ČL 6 najvyšší obsah uhlíka 65,54. Na druhej strane, síra bola prítomná v ligníne L-ČL 4 v podstatne nižšom množstve 0,16 %. Vanisperse CB má najvyšší obsah popola zo všetkých vzoriek 34,18 %, zatiaľ čo lignín L-ČL 6 má najnižší obsah 0,37 % (***Tab. 6***). Spalné teplo vzorky lignínu L-ČL 2 (25,88 MJ/kg) má v porovnaní s ostatnými najvyššiu energetickú hodnotu. Je to spôsobené uhlíkom, ktorý je v ňom najviac zastúpený, ale aj malým podielom popola vo vzorke. Nízky obsah síry, nízky obsah popola a najvyššia výhrevnosť predstavujú potenciál pre rôzne aplikácie.

Tab. 6 *Elementárna analýza prvkov, atómové pomery H/C, O/C, obsah popola (%) a hodnota spalného tepla (HHV)*

Vzorka	Elementárna analýza (%)					H/C	O/C	Popol (%)	Spalné teplo (HHV) (MJ/kg)
	H	N	C	S	O **				
Borresperse N *	4,65	0,14	44,11	6,49	21,27	0,11	0,48	23,34	18,36
Borrement Ca 120 *	5,35	0,14	46,63	5,62	28,96	0,12	0,62	13,13	19,46
Vanisperse CB *	4,08	0,12	52,54	2,96	6,11	0,08	0,12	34,18	20,61

Marasperse N-22 *	4,68	0,14	43,52	6,28	20,42	0,11	0,47	24,96	18,17
Orzan S *	5,05	0,09	45,42	5,15	33,46	0,11	0,74	10,83	18,30
DP – 02 *	4,38	0,16	42,86	5,12	27,84	0,10	0,65	19,64	17,31
DP – 03 *	5,08	0,14	48,12	7,15	17,10	0,11	0,36	22,41	17,99
L-ČL 2	5,93	1,18	63,64	0,49	28,34	0,09	0,45	0,43	25,88
L-ČL 3	4,62	0,28	55,68	3,91	31,65	0,08	0,57	3,85	23,62
L-ČL 4	5,70	1,47	64,25	0,16	25,51	0,09	0,40	1,52	17,65
L-ČL 5	5,19	0,28	59,75	2,03	32,75	0,09	0,47	3,39	23,62
L-ČL 6	6,17	1,20	65,54	0,04	27,05	0,09	0,41	0,37	23,61

* Komerčné ligníny Borresperse N, Borrement Ca 120, Vanisperse CB boli získané z Borregard LignoTech, Marasperse N-22 z Daishowa Chemical Inc, Orzan S z ITT Rayonier Inc, DP - 02, DP - 03 z Biotech

** L-ČL – ligníny pripravené z čierných lúhov s prideleným číselným označením (**Tab. 1**)

3.3 Vplyv podmienok pri zrážaní lignínu – pH a teplota

Na to aby sa porovnal vplyv podmienok (pH a teploty) počas zrážania lignínu sa urobil plánovaný experiment, z ktorého sa pripravilo 13 vzoriek lignínov. Vzorky sa pripravili zrážaním alkali-lignínu s kyselinou sírovou pri rôznych podmienkach. Menila sa hodnota pH a teplota, pri ktorej sa lignín pripravoval (***Tab. 3***). Výsledné vlastnosti pripravených lignínov sa ocharakterizovali a porovnali pomocou UV-Vis spektroskopie (***Tab. 7***). [5]

Tab. 7 *Výsledky UV-Vis na vzorkách lignínu z plánovaného experimentu*

Vzorka	Koncentrácia [g/l]	Nekonjugované OH skupiny [mmol/g]	Konjugované OH skupiny [mmol/g]	Celkové množstvo [mmol/g]
1	0,041	1,907	0,283	**2,190**
2	0,045	1,055	0,200	**1,255**
3	0,044	1,728	0,245	**1,973**
4	0,040	2,210	0,332	**2,543**
5	0,042	1,915	0,272	**2,188**
6	0,040	2,886	0,350	**3,235**
7	0,043	2,577	0,331	**2,907**
8	0,040	1,430	0,237	**1,667**
9	0,044	1,807	0,265	**2,072**
10	0,040	1,944	0,298	**2,242**
11	0,043	1,158	0,269	**1,427**
12	0,045	1,567	0,288	**1,856**
13	0,046	1,361	0,225	**1,585**

Z výsledkov merania vyplýva, že existuje závislosť medzi koncentráciou konjugovaných a nekonjugovaných fenolických OH skupín a podmienkami pri zrážaní lignínu. Z výsledkov plánovaného experiment vyplýva, že nekonjugované fenolické hydroxylové skupiny sú kvadraticky závislé od teploty počas zrážania. Na druhej strane, v prípade konjugovaných fenolických hydroxylových skupín existuje synergický efekt medzi teplotou a pH pri zrážaní.

3.4 Vplyv modifikácie na vlastnosti lignínu – zelený modifikátor (glycerín)

3.4.1 Základná charakteristika lignínov

Výťažky lignínov boli stanovené z absolútne suchého lignínu, ktorý bol vysušený v lyofilizátore do konštantnej hmotnosti. Popol sa stanovil pre zuhoľnatený zvyšok lignínov. Spalné teplo a výhrevnosť sa stanovili pomocou analytickej metódy – kalorimetrie.

Tab. 8 *Základná charakteristika lignínov (modifikovaných glycerínom)*

Vzorka	Výťažok [hmot. %]	Popol [hmot. %]	Spalné teplo [MJ/kg]	Výhrevnosť [MJ/kg]
FL	-	1,04	25,39	23,96
MOD - 0%	96,2	0,81	25,49	24,27
MOD1 - 5 %	92,5	0,92	25,51	24,36
MOD1 – 10 %	87,8	0,41	25,63	24,38
MOD1 - 15 %	84,1	0,78	25,68	24,56
MOD1 - 20 %	80,9	0,90	25,71	24,55
MOD1 - 25 %	76,7	0,64	25,72	24,59
MOD1 - 30 %	74,3	0,88	25,78	24,64

*MOD 0% = FL, pripravený pri podmienkach modifikácie, bez použitia modifikátora
MOD1 = Glycerín

Z výsledkov vyplýva, že lignín pripravený pri podmienkach modifikácie, ale bez použitia modifikátora má najväčší výťažok (96,2 %). Na rozdiel pri MOD1 pozorujeme klesajúci trend hmotnostného percenta výťažku aj napriek vyvyšujúcemu sa percentuálnemu prídavku modifikátora. Jedným z vysvetlení je, že na matricu lignínu sa nenafixovalo celé množstvo modifikátora a jeho účinok mohol spôsobiť rozpustenie časti lignínu, ktorý sa odstránil filtráciou.

Z ***Tab. 8*** vyplýva, že FL mal najvyšší obsah popola, resp. anorganických látok, konkrétne 1 % v porovnaní s modifikovanými lignínmi. V lignínoch pripravených modifikáciou s MOD1 nie je prítomná enormná zmena, čo svedčí o tom, že množstvo pridaného glycerínu neovplyvňuje tento parameter.

Hodnoty spalného tepla modifikovaných lignínov boli väčšie ako hodnota FL, z čoho vyplýva že modifikáciou lignínu sa získali ligníny s vyšším energetickým potenciálom ako bez použitia modifikácie. Pri MOD – 0% sa hodnota mierne líšila od FL, čiže teplota nemá až taký veľký vplyv na zmenu spalného tepla a výhrevnosti.

3.4.2 Stanovenie hydroxylových skupín pomocou UV-Vis

Z výsledných spektier sa určili maximá absorbancií pri dvoch analyzovaných vlnových dĺžkach (300 a 350 nm). Z výsledkov získaných pomocou UV-Vis spektroskopie vyplýva, že modifikácia a teplota na koncentráciu hydroxylových nevykazuje žiadnu významnú závislosť. Takéto výsledky sú významné z pohľadu hľadania vhodnej modifikácie hydroxylových funkčných skupín [5].

Tab. 9 *Výsledky charakterizácie lignínov (modifikovaných glycerínom) pomocou UV-Vis spektroskopie*

Vzorka	Nekonjugované OH skupiny [mmol/g]	Konjugované OH skupiny [mmol/g]	Celkové množstvo [mmol/g]
FL	1,14	0,22	1,36
MOD - 0%	1,07	0,27	1,34
MOD1 - 5%	0,79	0,25	1,04
MOD1 - 10%	0,93	0,26	1,19
MOD1 - 15%	0,86	0,24	1,10
MOD1 - 20%	0,74	0,28	1,02
MOD1 - 25%	0,74	0,25	0,99
MOD1 - 30%	0,83	0,25	1,09
MOD2 - 10%	1,25	0,24	1,50
MOD2 - 20%	1,31	0,25	1,56
MOD2 - 30%	1,40	0,25	1,65

*MOD = FL, pripravený pri podmienkach modifikácie, bez použitia modifikátora
MOD1 = Glycerín

3.4.3 Stanovenie termickej stability lignínu

Termická stabilita vzoriek lignínu bola analyzovaná v dvoch atmosférach, a to v oxidačnej (vzduch), a inertnej (dusík) atmosfére. Po spálení vzoriek sa získali TG krivky v obidvoch atmosférach. Prvou deriváciou TG kriviek sa pripravili DTG krivky, ktoré vyobrazujú priebeh rozkladu vzorky z pohľadu rýchlosti rozpadu. Termický rozklad vzorky poukazuje na termickú stabilitu lignínu. Pred začatím vyhodnotenia sa celková oblasť termického rozkladu vzorky rozdelila do viacerých teplotných intervalov. V každom jednom intervale sa merala maximálna teplota rozpadu vzorky v oxidačnej atmosfére (vzduch) a inertnej atmosfére (N_2). Nie každý lignín mal zastúpenie vo všetkých teplotných intervaloch, pretože niektoré píky boli veľmi malé a zmenou metódy: použitím rýchlejšieho ohrevu by sa nemuseli prejaviť (mohli by sa zanedbať). Preto sa za najpodstatnejšiu ukážku degradácie lignínu vybral práve najväčší pík, v najväčšom teplotnom intervale. Najväčší podiel úbytku vzorky lignínu nastáva pri vysokých teplotách.

Tab. 10 *Výsledky vzoriek lignínov (modifikovaných glycerínom) v oxidačnej atmosfére (vzduch) a v inertnej atmosfére (N_2)*

Vzorka	Oxidačná atmosféra					Inertná atmosféra		
	200-300 [°C]	300-400 [°C]	400-500 [°C]	500-800 [°C]	Úbytok [%]	200-300 [°C]	300-400 [°C]	Úbytok [%]
FL	256,1	x	x	525,2	-95,7	x	366,7	-57,6
MOD - 0%	258,2	x	x	556,1	-99,9	x	365,9	-57,3
MOD1 - 10%	257,3	382,4	x	557,2	-99,9	256,1	361,4	-53,2
MOD1 - 15%	257,6	x	x	558,5	-97,9	254,8	367,0	-57,7
MOD1 - 20%	257,7	x	422,1	559,3	-98,2	255,5	365,2	-54,6
MOD1 - 25%	256,3	380,9	x	561,0	-99,9	256,0	366,1	-54,6
MOD1 - 30%	256,1	382,5	x	560,1	-100	255,4	367,0	-53,8

*MOD = FL, pripravený pri podmienkach modifikácie, bez použitia modifikátora
MOD1 = Glycerín

V prípade MOD1 sa pozoruje mierne rastúci trend teploty s prídavkom modifikátora od 557,2 do 561,0 °C. Pri MOD1 sa teplota pri najväčšom úbytku skoro vôbec nelíši s teplotou FL (366,7 °C). Samotný modifikátor nemá veľký vplyv na termickú stabilitu vzoriek modifikovaných lignínov.

3.5 Vplyv rôznych modifikátorov na vlastnosti lignínu

3.5.1 Stanovenie Uv-Vis a FTIR analýzy

Pomocou UV-Vis sa stanovilo množstvo hydroxylových funkčných skupín vo vzorkách lignínov. Pomocou FTIR analýzy sa porovnali zmeny vo funkčných skupinách lignínu. Výsledky sú uvedené v ***Tab. 11***.

Modifikované vzorky sa porovnali s finálnym lignínom (FL), ktorý predstavoval 100 %. Vplyvom modifikácie sa mohla pozmeniť štruktúra a tým aj hodnota OH skupín. To viedlu k zníženiu koncentrácie OH skupín = pokles % (menšie percentuálne zastúpenie ako 100 %), alebo k zvýšeniu koncentrácie OH skupín = nárast % (väčšie percentuálne zastúpenie ako 100 %).

Tab. 11 *Výsledky charakterizácie lignínov (modifikovaných rôznymi modifikátormi) pomocou UV-Vis spektroskopie*

Vzorka	Nekonjugované OH skupiny [mmol/g]	Konjugované OH skupiny [mmol/g]	Celkové množstvo [mmol/g]	Porovnanie s referenčným lignínom FL (100%)
FL	1,579	0,334	1,913	100%

ACL 1	1,707	0,307	2,014	105%
ACL 2	0,868	0,164	1,032	54%
ACL 3	1,213	0,260	1,473	77%
ACL 4	1,437	0,269	1,706	89%
ACL 5	1,265	0,257	1,522	80%
DMPL 1	2,719	0,270	2,989	156%
SESAL 1	1,662	0,282	1,944	102%
SESAL 2	1,538	0,269	1,807	94%
SESAL 3	1,057	0,190	1,247	65%
SESAL 4	1,884	0,338	2,221	116%
SESAL 5	1,574	0,272	1,845	96%
SEANL 1	1,212	0,241	1,454	76%
SEANL 2	1,860	0,370	2,230	117%

Z výsledkov merania vyplýva, že došlo k zmenám koncentrácií nekonjugovaných a konjugovaných fenolických OH skupín vplyvom rôznych modifikácií voči finálnemu lignínu FL. Tým pádom sa zmenila aj celková koncentrácia OH skupín. Najväčšia hodnota negonjugovaných OH skupín vyšla pri vzorke DMPL 1 (2,719), v prípade konjugovaných pri vzorke SEANL 2 (0,370) s v prípade celkovej koncentrácie OH skupín pri vzorke DMPL 1 (2,989). Najväčší pokles nastal pri vzorke ACL 2 (- 46 %) voči FL a najväčší prírastok pri vzorke DMPL 1 (+ 56 %) voči FL. Pomocou FTIR analýzy sa zistilo, že došlo k zmenám tvaru spektier, čo predstavuje viaceré zmeny vo funkčných skupinách voči FL.

3.5.2 Stanovenie termickej stability lignínu

Termická stabilita vzoriek lignínu bola analyzovaná v dvoch atmosférach, a to v oxidačnej (vzduch), a inertnej (dusík) atmosfére. Použili sa rovnaké podmienky a vyhodnotenie ako v **kapitole 3.4.3**.

Tab. 12 *Výsledky vzoriek lignínov (modifikovaných rôznymi modifikátormi) v oxidačnej atmosfére (vzduch) a v inertnej atmosfére (N_2)*

Vzorka	**Oxidačná atmosféra**					**Inertná atmosféra**		
	200-300 [°C]	**300-400 [°C]**	**400-500 [°C]**	**500-800 [°C]**	**Úbytok [%]**	**200-300 [°C]**	**300-500 [°C]**	**Úbytok [%]**
FL	x	256,1	x	525,2	-95,7	x	366,7	-57,6
ACL 1	223,0	378,6	x	544,2	-92,7	226,5	370,4	-58,5
ACL 2	236,0	318,3	x	521,2	-96,4	235,7	332,4	-71,1
ACL 3	235,4	371,5	x	543,4	-94,1	239,2	370,7	-59,3
ACL 4	230,7	367,9	x	570,5	-95,9	230,1	371,5	-64,2
ACL 5	229,4	359,5	x	530,1	-96,3	225,1	373,7	-64,4
DMPL 1	172,9	x	410,4	525,3	-97,3	173,3	376,6	-60,2
SESAL 1	206,9	380,8	x	545,1	-100,0	60,3	407,3	-57,2

SESAL 2	x	376,8	x	548,7	-96,8	68,4	384,6	-56,2
SESAL 3	x	373,3	x	541,8	-98,2	66,9	406,8	-55,6
SESAL 4	x	378,4	x	561,7	-97,5	68,3	379,2	-54,6
SESAL 5	x	379,7	x	550,8	-96,3	241,6	379,3	-58,7
SEANL 1	256,2	x	x	554,8	-96,6	256,8	362,8	-57,8
SEANL 2	255,8	x	x	574,3	-96,6	259,8	361,9	-57,0

Z **Tab. 12** vyplýva, že vplyvom modifikácie sa zvýšila termická stabilita modifikovaných vzoriek lignínov, vzhľadom na FL. Najvyššie teploty úbytku možno pozorovať pri vzorke SEANL 2 s teplotou 574,3 °C v oxidačnej atmosfére (vzduch) a pri vzorkách SESAL 1 a SESAL 3 okolo 407 °C v inertnej atmosfére (N_2).

4 Poďakovanie

Táto práca bola podporená Agentúrou na podporu výskumu a vývoja pod číslami projektov APVV-22-0388 a APVV-22-0034.

5 Referencie

1. Zakzeski J, Bruijnincx PCA, Jongerius AL, Weckhuysen BM. The catalytic valorization of lignin for the production of renewable chemicals. Chem Rev 2010; 110: 3552–3599.

2. Nadányi R, Ház A, Lisý A *et al.* Lignin Modifications, Applications, and Possible Market Prices. Energies 2022, Vol 15, Page 6520 2022; 15: 6520.

3. Lebo SE, Gargulak JD, McNally TJ. Lignin. Encyclopedia of Polymer Science and Technology 2002;

4. Intapun J, Rungruang T, Suchat S, Cherdchim B, Hiziroglu S. The Characteristics of Natural Rubber Composites with Klason Lignin as a Green Reinforcing Filler: Thermal Stability, Mechanical and Dynamical Properties. Polymers 2021, Vol 13, Page 1109 2021; 13: 1109.

5. Majerčiak M., Nadányi R., Ház A., Smatanová D. EFFECT OF ISOLATION CONDITIONS ON LIGNIN PROPERTIES TOWARDS LIGNIN-BASED POLYMER MATERIALS. PMA 2023 & SRC 2023, Book of conference proceeding, 2023, 36–40.

6. Kočiš, J. 2013. Charakterizácia vlastností vyzrážaných lignínov. Diplomová téma. STU Bratislava, FCHPT – 13576 – 40586.

Sekce studentů doktorských studijních programů

„Vědy o živé přírodě a environmentální vědy“

Study of physicochemical properties of skin creams with the addition of liposomes

Kristýna Müllerová
Vojtěch Enev

Brno University of Technology,
Faculty of Chemistry,
Institute of Physical chemistry
Purkyňova 464/118, 612 00 Brno, Czech Republic
Kristyna.Mullerova@vut.cz

1 Introduction

The cosmetics industry offers many products for skin care and procedures for peeling, skin soothing, firming, protecting, and treating the skin. These products are easily available for everyday use. Their propagation is based on the effect produced by the active substance delivered to the skin. Spherical lipid vesicles, called liposomes, become very popular for transporting active substances to the skin. These particles in their structure can transport hydrophile, lipophile, and amphiphile molecules, which are widely used not just for the cosmetics industry [1; 2].

Quality control is important to ensure the efficacy and safety of a cosmetic product. Stability tests of a cosmetic product can be performed in real-time or under accelerated conditions. For stability testing under accelerated conditions, it is suitable to use, for example, the LUMiSizer analytical centrifuge with STEP-Technology. Quality tests should monitor stability and physical integrity under the specified conditions of storage, transport, and use, and should study chemical stability, microbiological stability, and compatibility between the cosmetic product and the container in which the product will be stored [3].

2 Experimental

2.1 Preparation of skin creams and liposomes

A sample of native skin cream was prepared, and then skin creams with 10%, 20%, and 30% addition of liposomal particles were prepared. All the raw materials used to prepare liposomes are shown in Table 1 and the raw materials for the preparation of creams are shown in Table 2. First was prepared material for the cream oil phase (jojoba oil, shea butter, olivoil emulsifier, and vitamin E). These compounds were put in the water bath temperate at 65 °C to melt. Next, the distilled water was measured and added to the water bath. The heated water was added to the complete melted oil phase and this mixture was homogenized at 5000 RPM for 5 minutes. A compound of glycerin and

xanthan gum was added to the prepared emulsion and was dispersed at 3000 RPM for 5 minutes. The mixture was left to cool slightly and then preservatives and essential oil were added. Again, the mixture was homogenized at 5000 RPM for 10 minutes.

Liposomes were prepared by the method of sonification by ultrasound homogenizer. Lecithin and cholesterol were put in the reagent bottle. Distilled water was added to this mixture. Vitamin E was dissolved in 4 ml of chloroform. The compound of vitamin and chloroform was added to the water, cholesterol, and lecithin in the reagent bottle. The mixture was sonicated by bar homogenizer with 70% efficiency for 15 seconds in 4 cycles. After sonification, the opened reagent bottle was put in a fume hood on a magnetic stirrer with a heating plate, which caused the chloroform to evaporate. Next, the skin cream was made – the preparation process was the same as the preparation of native skin cream. After the preparation of the lotion, the mixture was left to mildly cooled to a temperature of approximately 37 °C. At that temperature, 20 ml of the prepared liposome solution was gradually added to the cream while homogenizing with a dispersant at 3000 RPM for approximately 2 minutes.

Table 1 – The theoretical weighting for the preparation of liposomal particles with vitamin E. The total amount of creams was 120 g.

	10% liposomal	20% liposomal	30% liposomal
Lecithin	108.00 mg	216.00 mg	324.00 mg
Cholesterol	12.00 mg	24.00 mg	36.00 mg
Vitamin E	12.00 mg	24.00 mg	36,00 mg
Chloroform	1.2 ml	2.4 ml	3.6 ml
Distilled water	12.0 ml	24.0 ml	36.0 ml

Table 2 – The theoretical weighting for the preparation of skin creams. The total amount of cream was 120 g.

	Native cream	10% liposomal	20% liposomal	30% liposomal
Jojoba oil	12.00 g	12.00 g	12.00 g	12.00 g
Shea butter	12.00 g	12.00 g	12.00 g	12.00 g
Olivoil emulsifier	6.00 g	6.00 g	6.00 g	6.00 g
Vitamin E	12.00 mg	(–)	(–)	(–)
Distilled water	78.00 ml	66 ml	54 ml	42 ml
Glycerin	6,00 g	6.00 g	6.00 g	6.00 g
Xanthan gum	0.36 g	0.36 g	0,36 g	0.36 g
Essential oils				
Jasmine	25 drops	25 drops	25 drops	25 drops
Lavender	25 drops	25 drops	25 drops	25 drops
Rosewood	25 drops	25 drops	25 drops	25 drops
Preservatives				
Cosphagard elbe	2.40 g	2,40 g	2.40 g	2.40 g
Penthylen glycol	1.20 g	1.20 g	1.20 g	1.20 g
Liposomes + vit. E	0 ml	12 ml	24 ml	36 ml

2.2 Stability of prepared skin creams

All prepared samples were subjected to sedimentation analysis using a LUMiSizer analytical centrifuge. In all cases, the analysis was run at 4000 RPM for 5 hours and the measurements were performed in 4 cycles at a wavelength of 865 nm. All samples were run a total of four times to obtain more reliable data and measurements were performed at a laboratory temperature of 25 °C and subsequently at 37 °C, a temperature approximately equivalent to human body temperature. The stability study of prepared

Table 5 – The setup of the second step of the thixotropic test of skin cream.

Shear rate	200.0 s^{-1}	200.0 s^{-1}
Duration time	180 s	180 s
Delay time	5 s	5 s
Temperature	25 °C	37 °C

The third step of the experiment represented the behaviour of the cream after application and spreading on the skin, where again only gravity was applied to the sample.

Table 6 – The setup of the third step of the thixotropic analysis of skin cream.

Shear rate	0.1 s^{-1}	0.1 s^{-1}
Duration time	300 s	300 s
Delay time	1 s	1 s
Temperature	25 °C	25 °C

2.4 Characterization of liposomes

The prepared liposomes were measured on a ZetaSizer Nano ZS Mavern to study their stability and size for 12 weeks – the experiment was repeated every 4 weeks. From the prepared liposome solution, 1 ml was pipetted and diluted 100× with distilled water for analysis. The stability analysis of the liposomal particles was performed immediately after measuring their size, using the same sample. To measure the zeta-potential, a dip-electrode was dipped into the sample cuvette and the cuvette with the electrode was again carefully inserted into the instrument. The detailed setup of the methods is given in the tables below.

Table 7 – The setup of the measure of the particle size.

Index of refraction	Protein
Solvent	Water
Temperature	25 °C
Cell	Glass cuvette
Number of the measurements	9
Number of repeats in the measurement	12
beam position from the cuvette wall	1 mm

Table 8 – The setup of the measure of the zeta-potential.

Index of refraction	Protein
Solvent	Water
Temperature	25 °C
Cell	dip-electrode
Approximation	Smochulowsky
Repeats of the measurement	min. 10, max. 25
Number of the measurements	5

3 Results and Discussion

3.1 Long-term stability of skin creams

From the data obtained, the average stability values for each analysis interval were calculated. From the calculated values shown in Table 9, it can be seen that the native cream without the addition of liposomal particles showed the highest stability during the entire measurement interval at 25 °C, while the cream with 10 wt.% addition of liposomes in the aqueous phase was almost as stable as the native cream. The skin cream with a 30 wt.% addition of liposomes also showed good stability. The cream with 20 wt.% liposome addition showed the worst stability and the measured instability index values differed significantly from the other samples.

During the experiment at the laboratory temperature, it can be observed in general for all samples a continuous slow decrease of the instability index values, i.e., all samples showed an increase in stability during the 12 weeks. This phenomenon was likely due to the slight evaporation of water from the samples during handling experiments. Only the sample containing 10 wt.% liposomes when measured at 1 week and 12 weeks after preparation deviates from this trend, where a slight decrease in stability is evident. This change may have been due to the coalescence of air bubbles that entered the system during homogenization during sample preparation. It is also possible that the evaporated water that condensed on the plastic cap during storage came into contact with the lotion again (or leaked out during handling of the protective cap) and was dispensed into the measuring cuvettes with the sample during the experiments, which could have caused it to separate from the sample earlier and thus adversely affect the results.

Table 9 – Summary of average instability index values for all lotion samples at a temperature of 25 °C.

Age of skin cream	Native	10% liposomal	20% liposomal	30% liposomal
	Index of instability (–)			
1 day	0.014 ± 0.001	0.015 ± 0.003	0.054 ± 0.010	0.019 ± 0.003
1 week	0.012 ± 0.002	0.017 ± 0.003	0.041 ± 0.005	0.018 ± 0.003
4 weeks	0.011 ± 0.001	0.010 ± 0.002	0.037 ± 0,003	0.018 ± 0.003
12 weeks	0.010 ± 0,002	0.012 ± 0.004	0.025 ± 0.008	0.010 ± 0.002

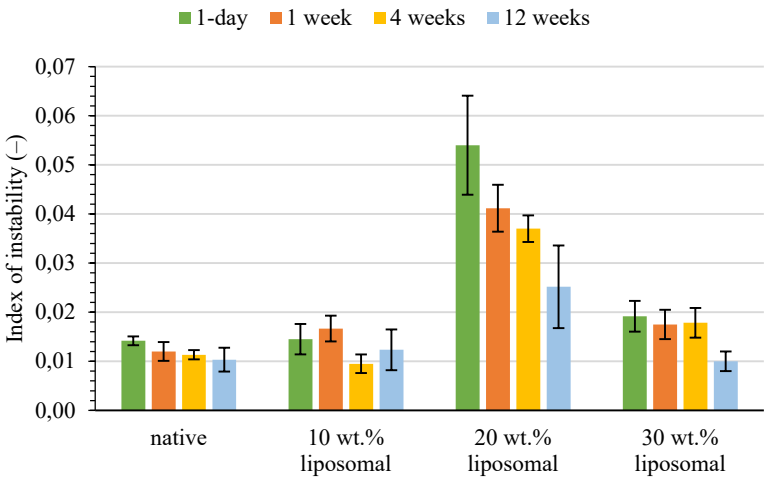

Figure 1 – Changes in the stability values of the samples at an interval of 12 weeks at 25°C.

Experiments carried out at an increased temperature of 37 °C show that the stability of skin creams decreases at higher temperatures. The average values of the instability indices are given in Table 10, and the calculated data show that the stability changed least in the case of the native lotion, whereas the sample with 20 wt.% liposome addition showed the greatest differences. The stability changes of all analysed samples are plotted graphically in Figure. 2.

The native sample without the addition of liposomes showed the least stability changes over time, although it did not show the highest stability immediately after preparation compared to the other samples. Furthermore, the sample with 30 wt.% addition of liposomal particles showed the least change in stability, although this sample showed the least stability at increased temperature at the beginning of the experiment. For these two samples, there was not only an increase in the instability index as there was for the other two samples, but the values changed in leaps and bounds over time. For the samples with 10 wt.% and 20 wt.% liposome addition, stability decreased with time, and phase separation occurred more readily, with a distinct layer of oily phase forming above the sediment. Since the increase in instability index values was predominantly due to the increase in the free phase, it can be assumed that evaporation of the free phase from the samples does not have a significant effect on the stability at increased temperatures.

Table 10 – Summary of the average instability index values for all lotion samples at a temperature of 37 °C.

Age of skin cream	Native	10% liposomal	20% liposomal	30% liposomal
	Index of instability (–)			
1 day	0.024 ± 0.002	0.015 ± 0.004	0.160 ± 0,014	0.217 ± 0.001
1 week	0.026 ± 0.002	0.025 ± 0.012	0.204 ± 0.002	0,205 ± 0.004
4 weeks	0.022 ± 0.003	0.026 ± 0.006	0.209 ± 0.001	0.203 ± 0.002
12 weeks	0.025 ± 0.006	0.042 ± 0.003	0.238 ± 0.012	0.213 ± 0.006

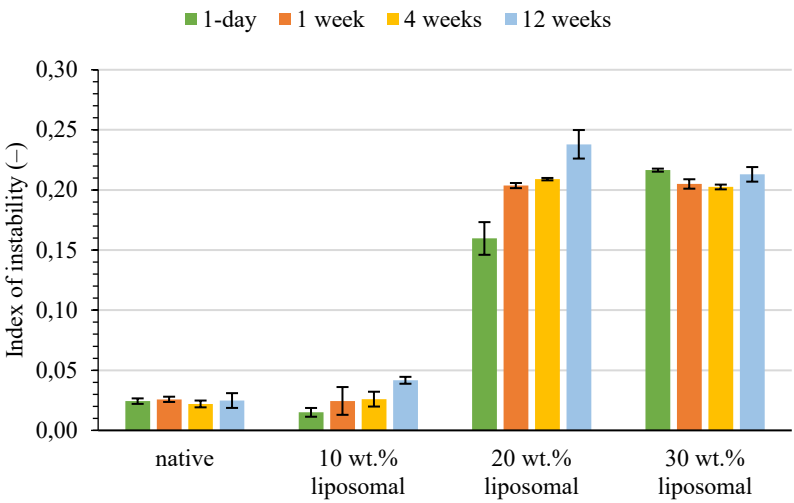

Figure 2 – Changes in the stability of the samples at an interval of 12 weeks at 37°C.

3.2 Rheological properties

All measured values were evaluated in Data Analysis software. After consultation, it was proposed to interleave the obtained data with the Cross model, from which zero and infinite viscosity values were subsequently obtained. This model was subsequently used for all measurements. The zero viscosity represents the viscosity that the sample would have if it were not subjected to any stress. It could be said to correspond to the viscosity of the sample during storage when only gravity is applied to the sample. Conversely, infinite viscosity can be thought of as corresponding to the viscosity of a sample that is subjected to an infinitely large shear force. In the case of lotions, it can be assumed that in practice the viscosity of the sample approaches this value when the lotion is spread on the skin.

The zero viscosity at 25 °C shows no common trend for all samples, which is evident from looking at the graphical representation of the changes in the values of this viscosity, see Figure 3. In the case of the native skin cream, there were step changes throughout the analysis, as well as in the case of the sample with 20 wt.% liposome addition, this dependence was plotted on the minor axis for clarity, as the values differed by an order of magnitude compared to the others at 4 weeks of age. In the case of the lotion with 10 wt.% liposomes, there was a slight increase in the zero viscosity values throughout the measurement period, and conversely, in the case of the sample with 30 wt.%, there was a decrease in these values throughout the experiment.

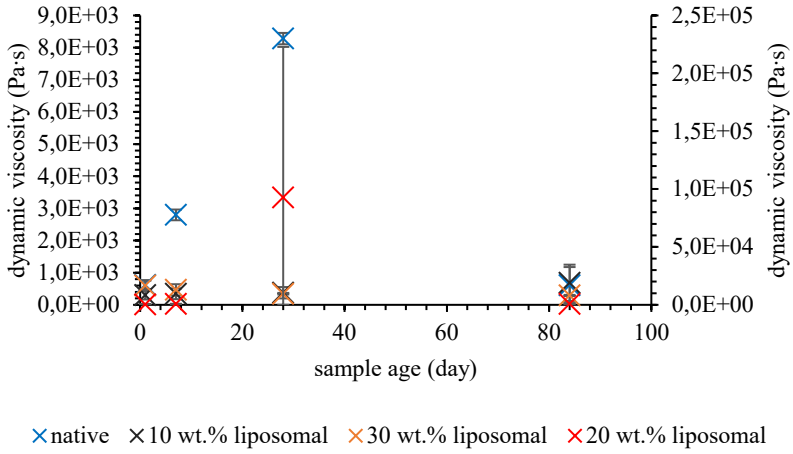

Figure 3 – Graphical representation of the changes in the values of zero viscosity at 25°C.

Figure 4 shows a summary of the average rounded values of the zero viscosities and the calculated standard deviations for measurements at 37 °C. It can be seen from the results that at increased temperatures, the native sample and the sample with the addition of 10 wt.% liposomes showed the largest variation in zero viscosity, in which case the zero viscosity increased with time. In the other two cases, the values varied in leaps and bounds.

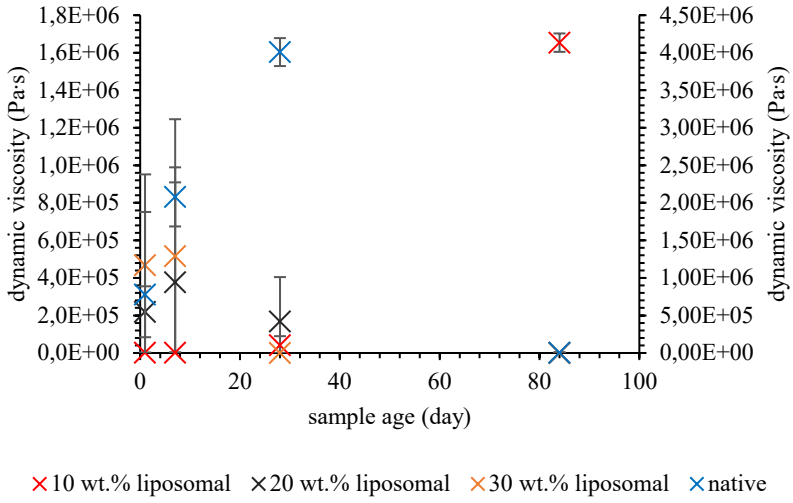

Figure 4 – Graphical representation of the changes of the values of zero viscosity at 37°C.

The infinite viscosity values obtained at laboratory temperature show that, as in the previous cases, the infinite viscosity values do not follow a common trend for all samples (Figure 5). Only in the case of the native sample, an increasing character can be seen throughout the experiment, whereas in the case of the sample with the addition of 20 wt.% liposomal particles, a decreasing character of the observed value throughout the measurements can be observed. The other two samples had higher values of infinite viscosity after the first week of the experiment than at the beginning of the measurement, but subsequently, the values decreased; after 12 weeks the value of the monitored parameter in the case of the sample with the addition of 10 wt.% liposomes increased significantly. In the case of the sample with 30 wt.% liposomes, the behaviour of the infinite viscosity was opposite after 12 weeks of measurements and a slight decrease in the values of the monitored parameter was observed.

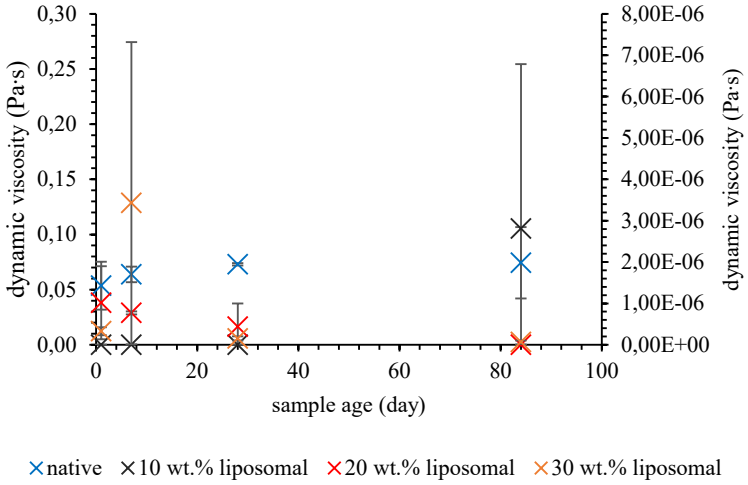

Figure 5 – Graphical representation of the changes in the value of infinite viscosity at 25°C.

The infinite viscosity at 37 °C can be considered as the viscosity of the samples when spread on human skin. The average values of these viscosities and the calculated standard deviations are plotted graphically in Figure 6 to better visualize the changes in values over 12 weeks. Only the native sample and the sample with 10 wt.% addition of liposomal particles showed a net increasing character of infinite viscosity throughout the experiment. For the other two samples, the values first decreased and then increased, and only the sample with 20 wt.% liposome addition did not increase to such an extent that the value at the beginning of the measurement was exceeded. The largest difference in values was observed for the sample with 10 wt.% liposome addition, which is plotted on the minor axis for clarity. From the measured values, it can be assumed that the cream with 10 wt.% liposomes is the best spreadable at the 1-day age of preparation as it shows the lowest infinite viscosity values. On the other hand, the cream with 30 wt.% liposome addition at an age of 12 weeks should be the least spreadable as it shows the highest infinite viscosity values.

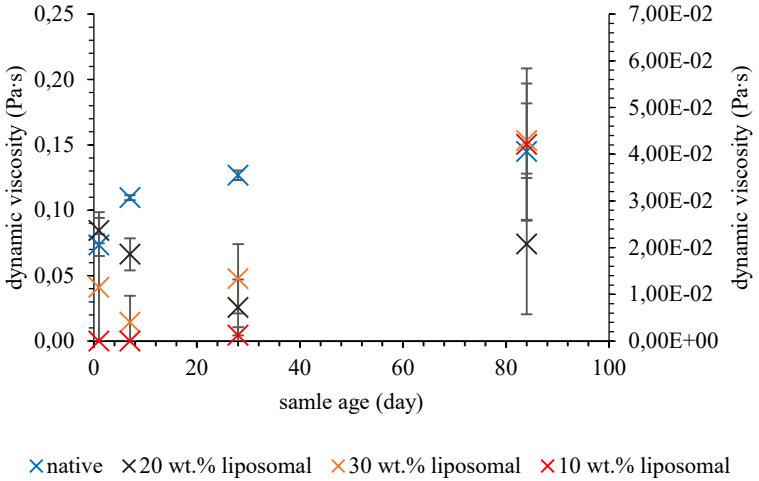

Figure 6 – Graphical representation of the changes in the value of infinite viscosity at 37°C.

From the measured data during the thixotropy study, the regeneration rate of the samples was calculated. Table 11 shows these values for measurements at 25°C. The results show that at the laboratory temperature at the beginning of the measurements, the native sample showed the highest regeneration rate; the lotions with the addition of liposomal particles regenerated their structure less well. In the long term, the regeneration rate tended to decrease. Conversely, in cases where a higher regeneration rate was observed, water may have evaporated from the sample during handling and storage. Conversely, the decrease in the regeneration capacity of the internal structure over time may have been due to changes that occurred in the structure of the samples. Coalescence of air bubbles and their disappearance during sample loading, slight phase separation of the emulsion base, condensation of evaporated water, oxidation of added liposomal particles, and possible microbiological activity may have occurred.

Table 11 – Values of the regeneration rate of the samples at 25°C.

	Regeneration rate			
Sample age	native	10 wt.% liposomal	20 wt.% liposomal	30 wt.% liposomal
1 day	47.78	40.05	38.91	44.24
1 week	50.34	39.97	38,55	44.68
4 weeks	40.09	33.20	41.88	44.83
12 weeks	37.29	32.38	36.31	31.27

The results for the increased temperature analysis show that the sample without liposomes again showed the highest rate of regeneration of the internal structure, this time at all measurement intervals (Table 12). It can be said that the rate of generation decreases with the age of the sample, which may be due to the same reasons already mentioned in

the previous paragraph. After the individual measurements were completed, in some cases a fine phase separation was visible on the sensor, suggesting that the aqueous phase was separated from the oily phase during the analysis. The separated oily phase could exhibit a higher stability on the sensor, which could increase the ability to regenerate the internal structure.

Table 12 – Values of the regeneration rate of the samples at 37°C.

	Regeneration rate			
Sample age	native	10 wt.% liposomal	20 wt.% liposomal	30 wt.% liposomal
1 day	40.15	33.12	35.98	33.01
1 week	35.75	32.81	28.93	21.32
4 weeks	34.78	29.89	24.57	24.76
12 weeks	31.49	29.16	24.66	28.48

3.3 Properties of liposomes

From the graphical dependence plotted in Figure 7, it can be seen that most of the particles are approximately in the range of 200 nm to 300 nm. These approximate size limits can be determined by the most prominent peaks, which reach their maximum at these values. In the case of the analysis at an age of 8 weeks, a small peak in the region around 40-60 nm can be observed, thus the system shows a higher polydispersity than the other measurements. It could be degrading liposomes, which break down into smaller particles due to oxidation of phospholipids, and thus release the encapsulated vitamin into the aqueous environment. Alternatively, it could be an error caused by a minor impurity in the system. When analysed after 12 weeks of age, the average particle size is again shifted to lower values, new particles may have formed in the system after degradation of some of the liposomes, or oxidation is not as pronounced.

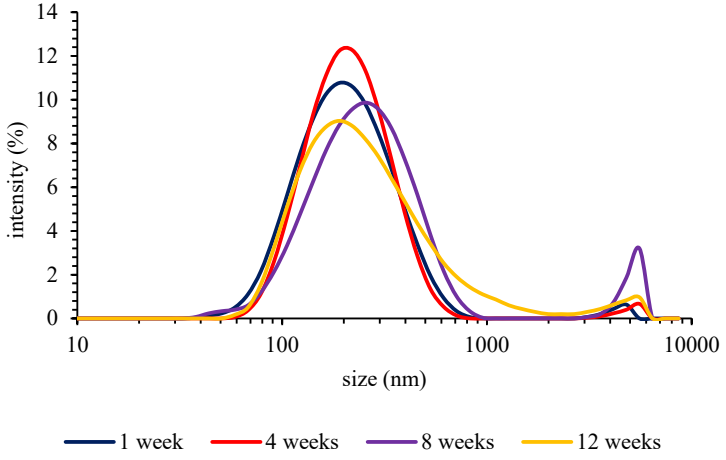

Figure 7 – Graphical dependence of intensity of light scattering on size of liposomal particles.

From the results, it is clear that except for the analysis at 8 weeks of age, the particles showed good stability as shown in Table 13. The particles can be considered very stable when the zeta-potential is higher than +30 mV or less than −30 mV. Samples can be considered most stable at 4 weeks of age and least stable at 8 weeks of preparation. Values after 8 weeks do not reach −30 mV, but since this stability limit is not fixed, the sample can still be considered stable. Changes in zeta-potential values correspond to changes in particle size studies.

Table 13 – Measured zeta-potential values during the 12-week observation period.

	1 week	4 weeks	8 weeks	12 weeks
Zeta-potential (mV)	(–)	−40.4	−30.4	−33.4
	−31.0	−40.8	−28.9	−32.9
	−33.0	−36.7	−29.5	−34.0
	−33.8	−35.9	−27.9	−32.9
	−32.4	−37.4	−26.9	−33.0
average of values	−32.5 ± 1.2	−38.2 ± 2.2	−28,7 ± 1.4	−33,2 ± 0.5

4 References

1. RÄHSE, Wilfried, 2020. Cosmetic creams: development, manufacture, and marketing of effective skin care products. Weinheim: Wiley-VCH. ISBN 978-3-527-81243-1.
2. AK, Mohiuddin. Skin Care Creams: Formulation and Use. OSP J Clin Trials: JTS-1-103. 2019, 22.
3. GUIDELINES ON STABILITY TESTING OF COSMETIC PRODUCTS [online]. B.m.: COSMETICS EUROPE – THE PERSONAL CARE ASSOCIATION. březen 2004. Dostupné z: https://www.cosmeticseurope.eu/files/5914/6407/8121/Guidelines_on_Stability_Testing_of_Cosmetics_CE-CTFA_-_2004.pdf

Lyophilisation as a useful method of carrier system preparation

Marek Řihák
Vojtěch Enev

Brno Univerzity of Technology,
Faculty of Chemistry,
Institute of Physical chemistry
Purkyňova 464/118, 612 00 Brno, Czech Republic
Marek.Rihak@vut.cz

1 Introduction

Hyaluronan is a widely used natural glycosaminoglycan which has a variety of functions in living organisms. According to its molecular weight it can be found in the intermolecular space as one of the main parts of the extracellular matrix as well as acts as one of the signalling molecules during cancer cells proliferation [1]. Although it has a strong hydrophilic character, advantageous equatorial position of polar groups offers a possibility for hydrophobic compounds to interact with hydrophobic carbon ring once the solvation shell is disrupted. The idea that hydrophobic interactions affect the conformation of the hyaluronan chain depending on the surrounding environment was explored by John E. Scott et al., who first published a paper in 1992 assigning the structure of hyaluronan in aqueous media to the shape of a double helix. In this paper authors also stated that hydrophobic domains can ensure an interaction of hyaluronan with other hydrophobic macromolecular compounds [2].

The idea of using freeze-drying to carefully reach the hydrophobic domain of hyaluronan was firstly mentioned in an article by Michalicová, Mravec and co. In this study, the authors focused on the accessibility of the hydrophobic domains of hyaluronan using the freeze-drying method. The fluorescence probes were used as a drug substitute which allowed them to observe the different behaviour of the probe in the system before and after lyophilisation. In addition, tert-butyl alcohol was used as a co-solvent which due to its –OH polar group is mixable with water but also makes suitable environment for dissolving a hydrophobic drug thanks to its quite large carbon skeleton. Tert-butyl alcohol in mixture with water further meets all requirements for a suitable solvent used for freeze-drying technique [3].

Freeze-drying is a gentle technique for drying samples that could be degraded by high temperatures. We are talking primarily about biological samples such as proteins, enzymes, saccharides etc. During the process of freeze-drying, samples in vacuum are frozen. As the temperature is then slowly raised, solvent sublimes from the sample. The

drying is divided into two parts; during primary drying nearly 95 % of water sublime, therefore the aim of secondary drying is to get rid of water residues, which are the molecules of water attached to the sample surface by adsorption. Once secondary drying is complete, the samples are fragile but retain their biological function [4].

2 Experimental

2.1 Freeze-drying

Solutions in beakers were covered with penetrated parafilm and placed on the shelfs of a freeze-dryer (SP VirTis Advantage Pro Freeze Dryer by AT). Freezing of the samples was caried out by gradually lowering the temperature to the final temperature of –15 °C at which the samples were left for 5 hours. During the primary drying the temperature was gradually raised (1 °C per 5 hours) as well as the pressure increased from 100 mTorr to 200 mTorr (20 mBar per 5 hours). During secondary drying the temperature was gradually raised to 25 °C with pressure of 800 mTorr. Lyophilized cakes were then transferred from beakers to vials and stored in a vacuum desiccator. Step-by-step freeze-drying process set up is shown below (Table 1 and Table 2).

Table 1: Thermal treatment of samples.

Step	T [°C]	Ramp [min]	Hold [min]	Step	T [°C]	Ramp [min]	Hold [min]
1	2	60	30	6	-15	30	300
2	0	15	30	7	–	–	–
3	-5	30	15	8	–	–	–
4	-10	30	60	9	–	–	–
5	-12	30	180	10	–	–	–

Table 2: Drying steps (primary and secondary drying of the samples).

Step	T [°C]	Ramp [min]	Hold [min]	Vacuum [mTorr]	Step	T [°C]	Ramp [min]	Hold [min]	Vacuum [mTorr]
1	-15	10	300	100	7	-5	60	600	300
2	-14	10	300	120	8	-2	60	600	400
3	-13	10	300	140	9	0	30	600	500
4	-12	10	300	160	10	5	60	300	600
5	-11	10	300	180	11	15	60	300	700
6	-10	10	300	200	12	25	120	450	800

2.2 Characterization of samples

Freeze-dried samples containing hyaluronan and drugs were dissolved in deionised water and measured using FS5 Edinburgh spectrofluorometer for (steady-state fluorescence) and Horiba Jobin Yvon Fluorocube (time-resolved fluorescence) whereby both were performed at a laboratory temperature.

Emission scan for steady-state fluorescence was set at 370–600 nm, with a variable excitation wavelength corresponding to the properties of individual samples. The individual wavelengths were obtained from excitation-emission spectra of drug samples dissolved in chloroform.

The time-resolved fluorescence measurement was performed with following set-up: 2048 channels, 10 000 counts, TAC 50 ns. From the results obtained from the mentioned spectra suitable diodes were selected for the characterization of each sample according to the value of the wavelength maximum of its fluorescence spectrum.

The samples were also measured using attenuated total reflectance FTIR technique using a Nicolet iS50 spectrometer (Thermo Fisher Scientific, Waltham, United States). Steady-state FTIR spectra were recorded over the rage of wavenumber from 4000 to 400 cm–1 with a resolution of 4 cm–1 and number of scans count of 64. The acquired data were analysed with a focus on the 1200–900 cm–1 wavenumber range, i.e. fingerprint region.

Tert-butyl alcohol residues were measured using the head-space solid phase microextraction with gas chromatography and mass spectrometry as a tandem analysing methods. A multicomposite fiber DVB/CAR/PDMS 50/30 mm was used for the microextraction with incubation at 40 °C and extraction at the same temperature. For the analyse Thermo Scientific TRACE 1310 Gas Chromatograph was used with TG-WAXMS (Thermo Scientific) column and following set-up: constat helium flow 1.0 mL·min–1 at 230 °C (to secure desorption from the fiber). Connected Mass Spectrometer ISQ LT with single quadrupole (Thermo Scientific) was used to determine solvent residues with characteristic value of m/z equal to 59. The data analysis was performed with NIST library.

3 Results and Discussion

Firstly, it must be said that since drug sample BI201335 could not be dissolved in a mixture of tert-butyl alcohol and water, it was excluded from the further examination. Secondly, all prepared samples were soluble as soon as they underwent lyophilization, which is the simplest confirmation of a successful preparation.

Due to the different fluorescence properties of each sample, each differed in the amount of drug studied. The concentration of drugs on the hyaluronic carrier is shown in the Table 3.

Table 3: Amount of drug per carrier.

Sample	Amount of drug per 1 g of carrier (mg)
1	1,75
2	2,6
3	1,0
5	0,8

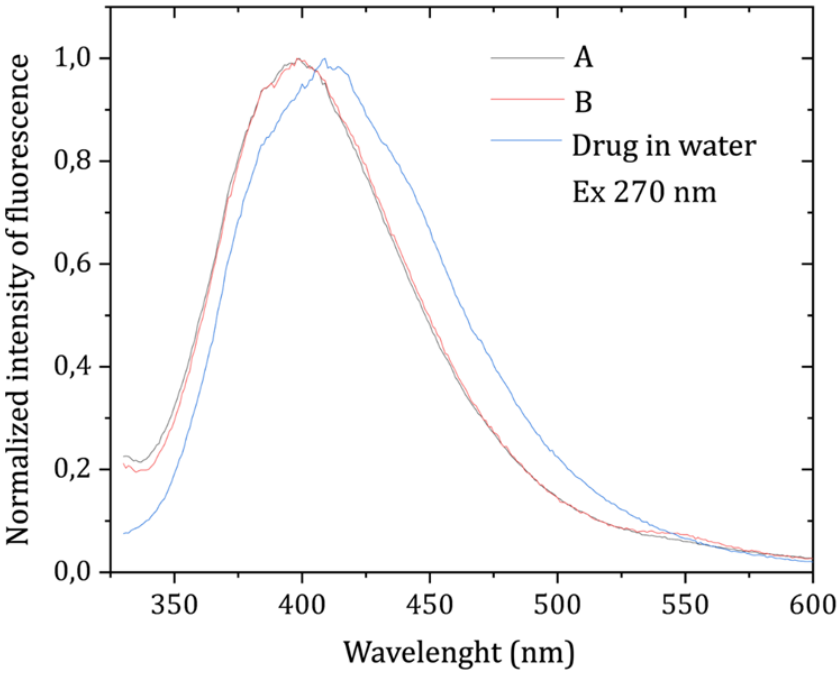

Figure 1: Fluorescence spectrum of sample 3 with noticeable blue-shift.

Steady-state fluorescence spectrum showed the desired shift of the peak emission intensity to the lower wavelengths (blue shift) compared to the emission spectrum of a drug in the aqueous environment. Although there is a significant difference of concentration of a drug carried by hyaluronan and of a drug that was able to dissolve in water (which from the hydrophobic character of the drug samples was very low), the blue shift indicates a change in the polarity of the environment in which the drug is located. The non-polar hydrophobic hyaluronan domains in which the drug is probably incorporated were made available thanks to tert-butyl alcohol cosolvent and freeze-drying process. Also increased intensity of fluorescence is a confirmation of a location of the drug in its preferred environment.

Time-resolved fluorescence was measured for drugs dispersed in water and for dissolved lyophilized systems. To dissolve at least a small amount of drugs in water, systems had to be kept on a laboratory magnetic stirrer for 5 days. After this time, it was possible to observe a significant aggregation of the drug in the upper part of the volumetric flask, which was caused by the drug trying to avoid contact with water. However, the fluorescence spectra indicate that at least a small part of the drug has been released into the aquatic environment.

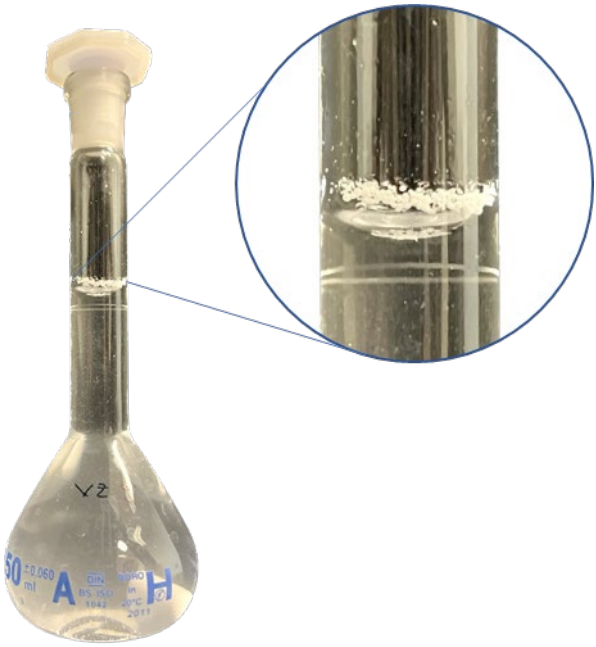

Figure 2: Volumeric flask with a significant affregate of drug.

While in the case of the drug itself in water the decay curve is nearly linear so when fitted only one lifetime of fluorescence per sample was gained, the freeze-dried systems show a quasi-exponential decrease, giving two lifetimes per sample. The first time could be considered as a lifetime of fluorescence of a drug in an aqueous environment whilst second time should be a confirmation of drug attached to the hyaluronan chain or of a drug incorporated into a polymeric coil. Since the measurement could be affected by light scattering, channel value 0,5 was set as a most probable value representing the scattering and was excluded to prevent the misinterpretation of the data. The most interesting results were in the case of sample 5 – as can be seen in Figure 3, fluorescence lifetime of a drug dispersed in water is very short whereas when lyophilized, significant second time was obtained proving that at least some drug particles are situated in a hydrophobic environment of hyaluronan domains.

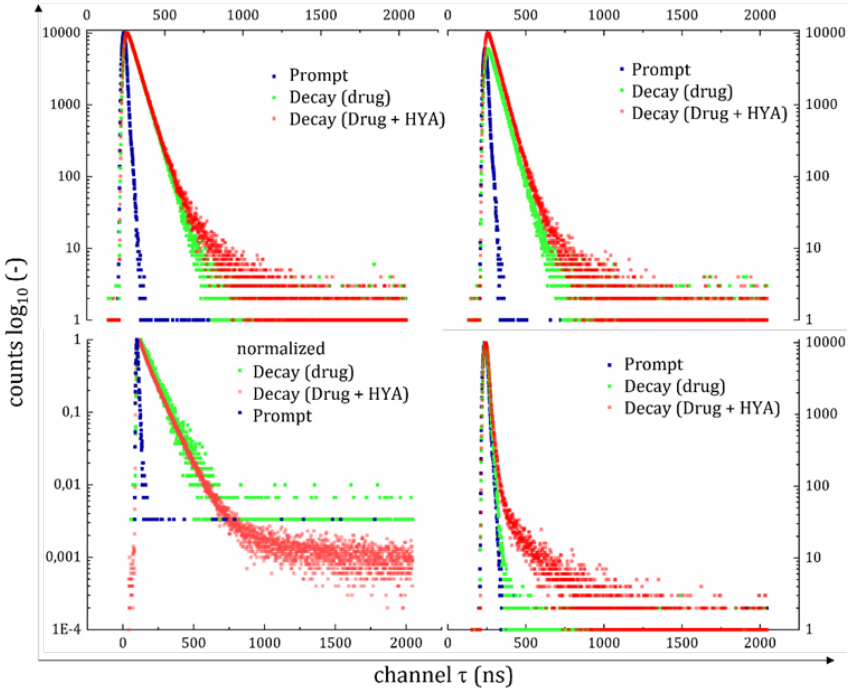

Figure 3: Fluorescence decays of lyophilised samples in comparison with drug alone.

Although sample 3 has an even higher second lifetime of fluorescence, it is uncertain whether the measurements for this sample are of indicative value since in the case of the drug in water the signal was so low that it was necessary to reduce the required number of counts. Nevertheless, the confirmation of a successful preparation of a carrier system in this case may not be the time difference but the fact, that once the system was lyophilized, the signal was much higher, corresponding to the higher concentration of the drug in the system caused by its incorporation into the hyaluronic carrier.

Table 4: Fluorescence lifetime of samples prepared in two batches and of the drug alone in water.

Sample 1			
	A	B	Drug in water
	time [ns]	time [ns]	time [ns]
scatter	0,01	0,01	0,01
t_1	1,57	1,58	1,62
t_2	4,59	5	-
Sample 2			
	A	B	Drug in water
	time [ns]	time [ns]	time [ns]
scatter	0,01	0,01	0,01
t_1	1,43	1,43	1,46
t_2	4,94	4,65	-
Sample 3			
	A	B	Drug in water
	time [ns]	time [ns]	time [ns]
scatter	0,8	1,0	0,03
t_1	5,2	5,4	5,02
t_2	47,1	56,9	-
Sample 5			
	A	B	Drug in water
	time [ns]	time [ns]	time [ns]
scatter	0,13	0,13	0,11
t_1	0,61	0,65	0,61
t_2	4,65	4,72	-

Lyophilized samples were also analysed by real time infrared spectroscopy with Fourier's transformation. These systems were compared with native lyophilized hyaluronan and native hyaluronan in a form of powder. Since the conformation of native hyaluronan in the form of powder is affected by air humidity which supports strong hydrophilic effect of the compound, the lyophilized systems underwent a process during which the solvation shell was disrupted causing the interruption of hydrogen bonds.

Formation of hydrogen bonds leads to prolongation of bonds such as, but not limited to, C–OH. Once the environment is unsuitable for forming these non-covalent interactions (when the samples are dried), the covalent bonds are shortened. In the presence of a hydrophobic drug, the hydrophobic effect is enhanced which leads to changes in the conformation of the whole polymeric chain in favour of orienting the hydrophobic parts together, also affecting the bonds previously participating in forming of hydrogen bonds.

As is shown in the Figure 2, lyophilized samples show a shift of absorption bends to higher values (higher energy), which is, as mentioned before, called a blue-shift. Attention was paid to the characteristic absorption band in the 1040 cm–1 wavelength region. This band corresponds to the C–OH valence vibration of primary alcohols and is characteristic for hyaluronan and easily recognizable since it is not affected by vibrations of the other groups. The shift is most significant for the samples with drugs which could be interpreted as another prove of the hydrophobic effect. Since the conformation of native hyaluronan in the form of powder is affected by air humidity which supports strong hydrophilic effect of the compound, the lyophilized systems underwent a process during which the solvation shell was disrupted causing the interruption of hydrogen bonds. Formation of hydrogen bonds leads to prolongation of bonds such as, but not limited to, C–OH. Once the environment is unsuitable for forming these non-covalent interactions (when the samples are dried), the covalent bonds are shortened. In the presence of a hydrophobic drug, the hydrophobic effect is enhanced which leads to changes in the conformation of the whole polymeric chain in favour of orienting the hydrophobic parts together, also affecting the bonds previously participating in forming of hydrogen bonds [5].

The concentration of residual tert-butyl alcohol was determined by head-space microextraction of thin layer. Due to the volatility of the solvent this method was an efficient way to analyse lyophilized samples and valuable data were obtained. The concentration of residues varies from 0,1 to 0,2 wt. % which is higher than was expected and will therefore be the subject of further studies. In the chromatograms we can also see a distinct peak with a retention time of 6,24 seconds. This peak could correspond to compounds formed by microbial activity on hyaluronan.

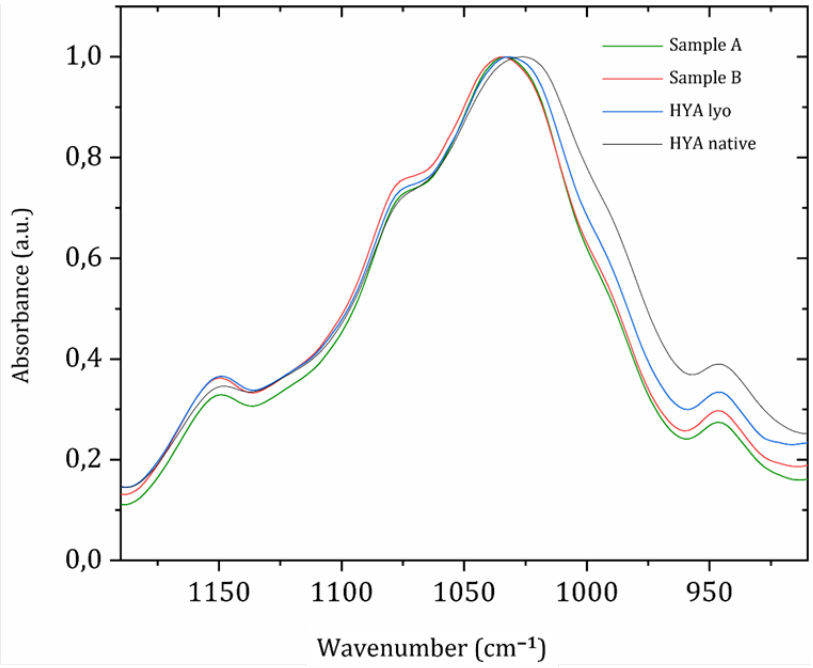

Figure 4: FTIR spectrum of sample 3 in comparison to lyophilised hyaluronan and native hyaluronan in the form of powder with a visible blue-shift.

4 References

1. HARDINGHAM, Tim, 2004. Chapter 1 - Solution Properties of Hyaluronan. In: Chemistry and Biology of Hyaluronan [online]. 1. Manchester: Elsevier Science Ltd, s. 1-19 [cit. 2022-09-19]. ISBN 9780080443829. From: https://doi.org/10.1016/B978-008044382-9/50032-7
2. SCOTT, J. E., 2007. Secondary Structures in Hyaluronan Solutions: Chemical and Biological Implications. Ciba Foundation Symposium 143 - The Biology of Hyaluronan [online]. Chichester, UK, 2007-09-28, 6-20 [cit. 2023-02-27]. Novartis Foundation Symposia. ISBN 9780470513774. From: doi:10.1002/9780470513774.ch2
3. MICHALICOVÁ, Petra, Filip MRAVEC, Miloslav PEKAŘ a Bing XU, 2017. Fluorescence study of freeze-drying as a method for support the interactions between hyaluronan and hydrophobic species. PLOS ONE [online]. 2017-9-8, 12(9) [cit. 2023-10-11]. ISSN 1932-6203. From doi:10.1371/journal.pone.0184558
4. NOWAK, Dorota a Ewa JAKUBCZYK, 2020. The Freeze-Drying of Foods—The Characteristic of the Process Course and the Effect of Its Parameters on the Physical Properties of Food Materials. Foods [online]. 9(10) [cit. 2023-10-11]. ISSN 2304-8158. From: doi:10.3390/foods9101488

5. HEIKO A. SCHIFFTER, Heiko A. a Sebastian VANHOFF, 2009. The determination of structural changes of biopharmaceuticals during Freeze-Drying using Fourier Transform Infrared Spectroscopy. European Pharmaceutical Review [online]. 2009(2), 1-5 [cit. 2023-04-12]. From: https://www.europeanpharmaceuticalreview.com/article/944/the-determination-of-structural-changes-of-biopharmaceuticals-during-freeze-drying-using-fourier-transform-infrared-spectroscopy/

Sekce studentů doktorských studijních programů

„Materiálové vědy“

Printed colorimetric amine indicator for food packaging

Vojtěch Dobiáš[1]
Michal Veselý[1]

[1]*Institute of Physical and Applied Chemistry, Faculty of Chemistry, Brno University of Technology, Purkyňova 464/118, 612 00 Brno, vojtech.dobias@vut.cz*

1 Introduction

Food poisoning is an unpleasant experience. An estimated 600 million people fall ill from contaminated food every year [1]. Systems to reduce the probability of the food becoming dangerous for human consumption have been developed (e.g.: Hazard Analysis Critical Control Point (HACCP) [2] or various methods of extending the food shelf-life, such as vacuum or modified atmosphere packaging).

Among other compounds, ammonia and amines are evolved as a product of protein decomposition by bacteria during the food spoilage [3]. Amines are organic compounds with an NH_2 group which renders amines basic substances. Therefore, amines can affect the pH of a solution. There has been ongoing research on smart food packaging indicators based on a pH change [4–7]. However, amines can also specifically react with ninhydrin forming a colored substance.

This contribution describes an indicator based on the reaction between amines and ninhydrin. The indicator design lies in ninhydrin–hydroxypropyl cellulose solution printed on a PET foil. The printed indicator is also covered with a UV-curable coating that should act as a barrier between the indicator and the food inside the packaging, reducing the risk of food contamination.

2 Experimental

2.1 Chemicals

Following chemicals were used in this work: ninhydrin (Sigma-Aldrich), hydroxypropyl cellulose (Kremer Pigmente GmbH & Co. KG), butylamine (Sigma-Aldrich), isopropanol (Ing. Petr Švec – PENTA s.r.o.), UV coating Packcure Secure Opaque white CPY90100 (FlintGroup), deionised water

2.2 Preparation of aqueous butylamine solution

3.22 g of butylamine was added in to 50 ml of deionized water. The solution was mixed and stored in a volumetric flask in the dark at room temperature.

2.3 Preparation of amine indicator polymer printing mixture

An aqueous solution of ninhydrin with concentration 0.2 % (w/w) was prepared by adding the weighted amount of ninhydrin to deionized water. After dissolution of ninhydrin, hydroxypropyl cellulose was added so that the final solution was 5 % (w/w) with respect to hydroxypropyl cellulose. The final mixture was kept in a plastic container in the dark at room temperature.

2.4 Amine indicator printing

The amine indicator printing mixture was printed on a PET foil Optimont® 501 (Bleher) using Mayer's rod (Industrial Physics) and TQC automatic coater (Industrial Physics). The PET foil was cleaned with isopropanol before printing. The thickness of the wet printed layers was 30 μm. The printed layers were dried at 60 °C for 5 minutes in laboratory hot air dryer UF110 (Memmert). The dried indicators were then covered with a UV-curable coating using screen printing machine SD 05 (RokuPrint) using screen 180-27Y (SERVIS CENTRUM a.s.). The coating was then cured for 19 minutes using a UVC lamp (ULTRALIGHT AG). The distance between the coating and the source of irradiation was set to 40 cm.

2.5 Amine sensitivity

The indicator solution on a PET foil was placed inside the measurement apparatus, which is shown in Figure 1. The indicators were cut to 2 cm squares and fixed onto alumina ceramic plates or microscopic glass slides. The fixed indicators were placed inside the measurement apparatus. The schematic view in Figure 2 illustrates the measurement setup in more detail. Reflectance probe was inserted into the apparatus and 1 ml of aqueous butylamine solution was injected into the apparatus. At this point, the stopwatch was started.

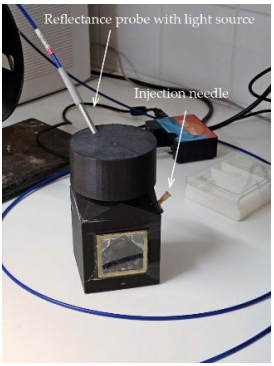

Figure 1: Amine sensitivity measurement apparatus

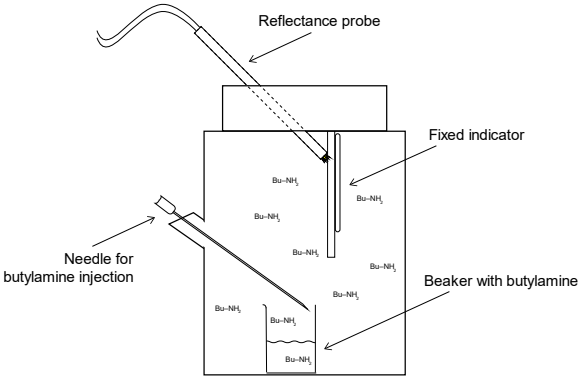

Figure 2: Schematic view of the measurement apparatus

2.6 Reflectance spectra measurement

Reflectance spectra were measured with spectrophotometer USB 650 UV (OceanInsight). The spectrophotometer was calibrated against white reference: clean alumina ceramic plate for polymer indicators with no coating and against UV coating for coated polymer indicators. During the exposure to butylamine, reflectance spectra were captured every 20 minutes. The $L^*a^*b^*$ values were calculated by the spectrophotometer's software.

Reflectance spectra were converted to spectra of optical densities by using formula (1):

$$D_\lambda = -\log\left(\frac{R_\lambda}{100}\right) \quad (1)$$

,where D_λ is spectral optical density and R_λ is spectral reflectance.

The color difference value ΔE^*_{ab} was calculated using formula (2) [8]:

$$\Delta E^*_{ab} = \sqrt{(\Delta L^*)^2 + (\Delta a^*)^2 + (\Delta b^*)^2} \quad (2)$$

,where ΔE^*_{ab} is color difference value, ΔL^* , Δa^* , Δb^* is the difference between L^* , a^* , b^* values of two colors.

3 Results and discussion

The uncoated printed amine indicator is sensitive to butylamine as can be seen from the change of optical density spectra in Figure 3. The color change is easily distinguished by naked eye in 80 minutes in a direct comparison. This color difference is characterized by value of $\Delta E^*_{ab} = 7$. The color change is visualized in Figure 4. Figure 5 illustrates how the color difference value changed during the butylamine exposure.

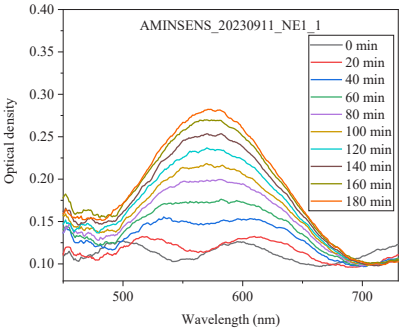

Figure 3: Optical density spectra for printed amine indicator with no coating

Figure 4: Visualization of the indicator's color change during the butylamine exposure

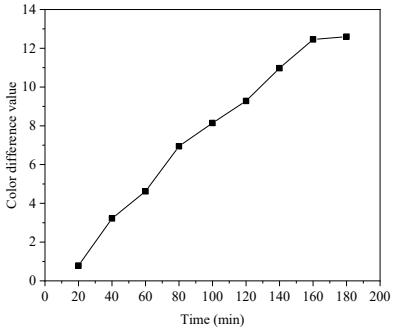

Figure 5: Color difference value vs time of butylamine exposure

From the optical density spectra in Figure 6, it can be concluded, that the UV coating blocks the butylamine molecules from reaching the printed indicator, as no color change was observed. This is in contrast with earlier findings by our group, where the UV curable coating was permeable for oxygen. Butylamine is larger molecule, compared to oxygen, which is probably the reason why butylamine does not penetrate the coating.

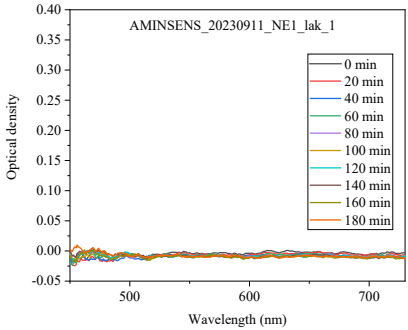

Figure 6: Optical density spectra for UV coating covered printed amine indicator

4 Conclusion

An amine indicator for food packaging was prepared by printing the indicator solution on a PET foil. The indicator successfully reacted to butylamine with visible color change that can be distinguished by the naked eye in 80 minutes in direct comparison. However, when the indicator is coated with an UV curable coating, no color response was observed. Further research on suitable indicator coatings is needed to ensure food safety of the packaged food.

References

[1] Food safety, (n.d.). https://www.who.int/news-room/fact-sheets/detail/food-safety (accessed November 26, 2023).

[2] HACCP Principles & Application Guidelines, FDA. (2023). https://www.fda.gov/food/hazard-analysis-critical-control-point-haccp/haccp-principles-application-guidelines (accessed November 29, 2023).

[3] A.E.-D.A. Bekhit, B.W.B. Holman, S.G. Giteru, D.L. Hopkins, Total volatile basic nitrogen (TVB-N) and its role in meat spoilage: A review, Trends Food Sci. Technol. 109 (2021) 280–302. https://doi.org/10.1016/j.tifs.2021.01.006.

[4] A. Pacquit, K.T. Lau, H. McLaughlin, J. Frisby, B. Quilty, D. Diamond, Development of a volatile amine sensor for the monitoring of fish spoilage, Talanta. 69 (2006) 515–520. https://doi.org/10.1016/j.talanta.2005.10.046.

[5] B. Kuswandi, Jayus, T.S. Larasati, A. Abdullah, L.Y. Heng, Real-Time Monitoring of Shrimp Spoilage Using On-Package Sticker Sensor Based on Natural Dye of Curcumin, Food Anal. Methods. 5 (2012) 881–889. https://doi.org/10.1007/s12161-011-9326-x.

[6] Q. Ma, L. Wang, Preparation of a visual pH-sensing film based on tara gum incorporating cellulose and extracts from grape skins, Sens. Actuators B Chem. 235 (2016) 401–407. https://doi.org/10.1016/j.snb.2016.05.107.

[7] I. Choi, J.Y. Lee, M. Lacroix, J. Han, Intelligent pH indicator film composed of agar/potato starch and anthocyanin extracts from purple sweet potato, Food Chem. 218 (2017) 122–128. https://doi.org/10.1016/j.foodchem.2016.09.050.

[8] R.W.G. Hunt, The Reproduction of Colour, Fifth editon, Fountain Press, 1995.

Acknowledgement

This research was supported by the project OP PIK–Aplikace CZ.01.1.02/0.0/0.0/20_321/0024435 funded by the Ministry of Industry and Trade of the Czech Republic.

Delignification of wheat straw using deep eutectic solvents-like mixtures

Veronika Jančíková
Michal Jablonský
Katarína Voleková

Brno Univerzity of Technology,
Faculty of Chemistry,
Institute of Physical chemistry
Purkyňova 464/118, 612 00 Brno, Czech Republic
veronika.jancikova@stuba.sk

1 Introduction

The growing demand for energy and materials in modern society is pushing scientific research to find new alternative sources to traditional fossil raw materials. The use of biomass represents the use of an alternative with a lower negative impact on the environment.

Lignocelluloses are considered as the most promising starting material to express the concept of biorefinery. These such as agricultural residues, forest residues, herbaceous and woody energy crops and specialty crops are renewable and inexpensive with an annual production of 200 gigatons per year. This fact can make them an alternative to fossil resources. Efficient recovery of the valuable content in lignocellulosic biomass requires pretreatment techniques capable of efficiently fractionating the biomass to overcome the defiant properties of the substances of this matrix[1,2].

A relatively new class of green solvents that has been addressed by many authors are deep eutectic solvents-like mixtures (DES-like mixtures)[3]. The replacement of commonly used solvents by green solvents is a very broad area of research and development. These solvents are rapidly being developed and used as alternative solvent systems for the processing of lignocellulosic materials. Nowadays, the isolation of fibres from annual plants is becoming a key issue due to the availability of woody biomass[4]. Research has shown that DES-like mixtures can be used to dissolve and hydrolyze certain biomass components (e.g., lignin), under mild conditions that prevent further degradation[5].

2 Experimental

2.1 Design of a rotation experiment

As a source of biomass, we chose wheat straw from Slovakia, specifically from the vicinity of Bratislava. The wheat straw was cleaned of external dirt, leaves and rings and then cut into 2 to 3 cm pieces. The input biomass was analysed for its chemical composition (lignin, dry matter, cellulose, holocellulose, ash and extractives content).

For delignification of wheat straw, we used DES-like mixtures in the composition of choline chloride/lactic acid in a molar ratio of 1:5. The preparation of this solvent was carried out as follows: a pre-calculated amount of choline chloride and lactic acid was weighed into a round bottom flask. The mixture thus prepared in the flask was placed in a water bath, which was run with constant stirring for about 30 minutes at 80°C until a homogeneous clear liquid was obtained.

To perform the delignification, we prepared the rotary experiment in advance. By this term we mean the experiments of a given experiment arranged in a specific way, and by using it we can evaluate the experiment as efficiently as possible mathematically and statistically[6].

Table 1: Proposed delignification conditions for the rotary experiment

Number of experiments	Delignification temperature (°C)	Delignification time (min)	Biomass to solvent ratio (g/g)
1.	96	97	1:12
2.	144	97	1:12
3.	96	204	1:12
4.	144	204	1:12
5.	96	97	1:30
6.	144	97	1:30
7.	96	204	1:30
8.	144	204	1:30
9.	80	150	1:17
10.	160	150	1:17
11.	120	60	1:17
12.	120	240	1:17
13.	120	150	1:10
14.	120	150	1:60
15.	120	150	1:17
16.	120	150	1:17
17.	120	150	1:17
18.	120	150	1:17
19.	120	150	1:17
20.	120	150	1:17

2.2 Delignification procedure

The next step in our work was to perform delignification on the characterized biomass. For delignification, we chose a constant mass of a.s. biomass namely 20 g. Then, according to the rotary experiment, we prepared a suitable amount of DES-like mixtures

(200 g), which were put into the digester along with the biomass. We used the temperature and delignification time according to the rotary experiment (Table 1). In total, we performed 20 experiments, which yielded pulp filter cakes after filtration under reduced pressure. We set aside the residual leachate in empty dust trays. We also filtered the leachate from the dust collectors after a few days to obtain the filter cake of lignin. We dried the filter cakes of fibers in a drying oven to a constant weight to determine the pulp yield after delignification.

Table 2: Characterization of the pulp after rotary experiment

Number of experiments	Cellulose (%)	Holocellulose (%)	Ash (%)	Lignin (%)	Yield after delignification (%)
1.	65.65	72.34	2.81	20.05	69,9
2.	53.98	66.97	4.28	28.77	53,6
3.	57.27	72.12	4.39	22.67	63,2
4.	52.75	62.55	4.75	33.02	58,2
5.	50.52	71.44	6.06	17.98	60,6
6.	74.44	72.67	4.53	22.95	50,4
7.	51.75	71.97	3.91	22.63	57,8
8.	65.93	71.28	3.31	24.54	51,3
9.	45.01	69.61	3.99	21.56	74,4
10.	43.77	59.17	5.35	35.49	56,8
11.	58.18	79.61	3.05	19.69	52,3
12.	58.18	70.85	4.04	19.22	51,3
13.	53.21	66.66	5.08	27.58	58,2
14.	69.53	80.30	4.26	16.13	48,1
15.	60.88	74.96	4.99	19.34	53,2
16.	59.81	77.66	4.83	18.8	55,2
17.	58.89	75.18	4.41	18.69	53,0
18.	59.39	73.30	4.07	19.21	55,4
19.	61.29	74.95	4.35	18.97	53,0
20.	58.61	76.70	4.33	19.89	53,7

2.3 Evaluation of the rotation experiment

Table 3: Calculated optimal conditions for delignification

Monitored substance content in biomass	Cellulose (%)	Holocellulose (%)	Ash (%)	Lignin (%)
Ideal yield (%)	67.74	80.31	1.55	16.44
Temperature(°C)	143	120	80	111
Time (min)	240	150	60	60
Biomass to solvent ratio (g/g)	1:58	1:17	1:10	1:27

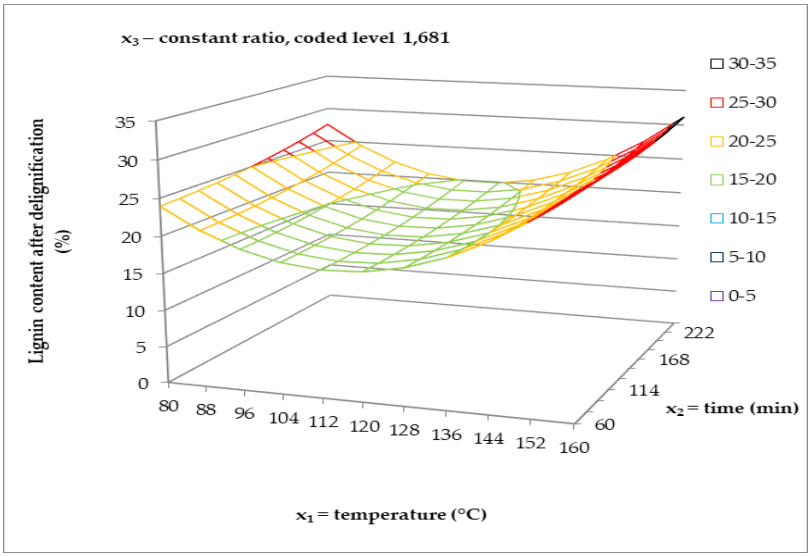

Figure 1: Dependence of lignin content on temperature and time of delignification

2.4 FT-IR and SEM analyses

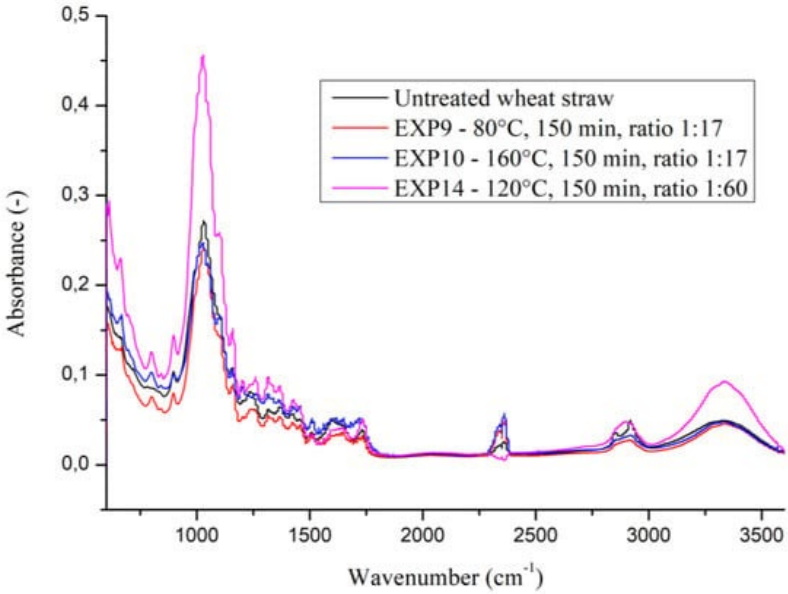

Figure 2: FT-IR spectra of the untreated wheat straw and samples 9,10, and 14 after delignification

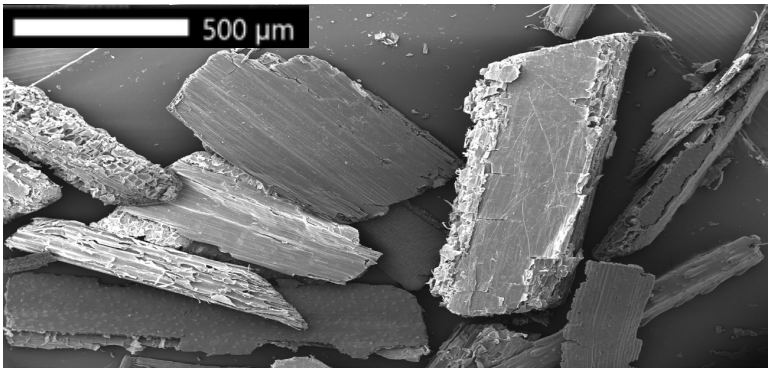

Figure 3: Image of the original biomass at magnification 30X

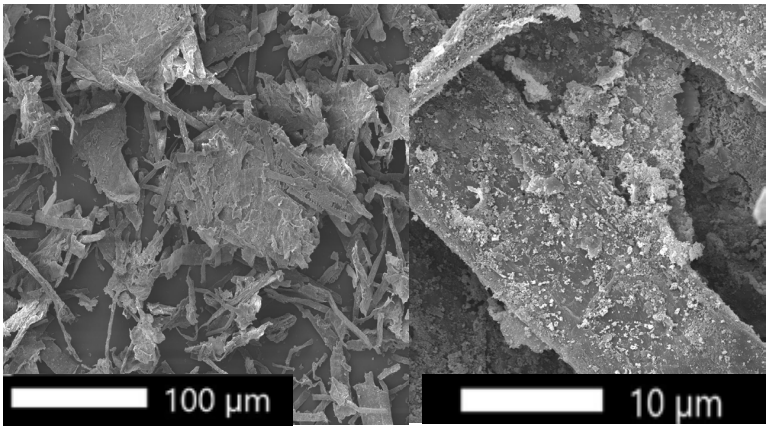

Figure 4: Images of the fibers after delignification (a) experiment 4; (b) experiment 10 at magnifications 100X (a) and 1000X (b)

3 Results and Discussion

The percentage of lignin remaining in the samples after delignification varied between 16.13% and 35.49%, while the cellulose content fell within the range of 43.77% to 69.53%. To pinpoint optimal conditions for delignification, we performed calculations. The ideal lignin content of 16.44% was achieved at a temperature of 111 °C, a duration of 60 min, and a biomass to solvent ratio of 1:27.

Although we obtained higher lignin contents in our delignification and lower yields compared to other studies, the use of green solvents is still preferable alternative for delignification of wheat straw or other annual plants. Their properties are an advantage in terms of use as they are non-flammable, biodegradable, environmentally friendly or economically advantageous.

4 References

1. KUMAR, B., BHARDWAJ, N., AGRAWAL, K., CHATURVEDI, V., VERMA, P. Current perspective on pretreatment technologies using lignocellulosic biomass: An emerging biorefinery concept. FUEL PROCESSING TECHNOLOGY. 2020, n.199, p. 106244. DOI: 10.1016/j.fuproc.2019.106244.
2. SCELSI, E., ANGELINI, A., PASTORE, C. Deep eutectic solvents for the valorisation of lignocellulosic biomasses towards fine chemicals. BIOMASS. 2021, n.1, p.29-59. DOI: 10.3390/biomass1010003.
3. JANČÍKOVÁ, V., JABLONSKÝ, M., VOLEKOVÁ, K., ŠURINA, I. Summarizing the effect of acidity and water content of deep eutectic solvent-like mixtures- A review. ENERGIES. 2022, n.15, p. 9333. DOI: 10.3390/en15249333.
4. JANČÍKOVÁ, V., JABLONSKÝ, M. Delignification of hemp stalk using a low transition temperature mixture composed of choline chloride and lactic acid. BIORESOURCES. 2022, n.17, p. 1232-1240. DOI: 10.15376/biores.17.1.1232-1240.
5. MAJOVÁ, V., STRIŽINCOVÁ, P., JABLONSKÝ, M., ŠKULCOVÁ, A., VRŠKA, M., MALVIS ROMERO, A. Deep eutectic solvents: Delignification of wheat straw. THE WORLD SUSTAINABLE ENERGY DAYS. 2017.
6. ALEXY, P., VISELKA, M. Základy plánovania a vyhodnocovania experimentov a Programový modul STATIS pre MS EXCEL 5.xx až 7.0. Bratislava: Chemickotechnologická fakulta, Slovenská Technická Univerzita Bratislava, 1998.

Photocatalytic layers of graphitic carbon nitride and siloxane binder

Sylvia Patakyová
Petr Dzik

Brno Univerzity of Technology,
Faculty of Chemistry,
Institute of Physical Chemistry
Purkyňova 464/118, 612 00 Brno, Czech Republic
Sylvia.Patakyova@vut.cz

1 Introduction

Due to the threat of an impending energy crisis and environmental problems due to the overuse of fossil fuels and the increase in CO_2, it is necessary to develop environmentally friendly technologies capable of replacing energy-intensive processes. One of these technologies is photocatalysis, which can convert solar energy into chemical energy and, thanks to suitable photocatalysts, can split water, convert CO_2, and degrade organic pollutants [1]. Most of the available conventional photocatalysts are precious metals or their oxides, which have limited practical applications due to their cost, lower photocatalytic activity, or because of the risk of environmental pollution. This is the reason why carbon-based photocatalysts are gradually being used to replace conventional photocatalytic materials or to serve as carriers to enhance activity [2].

Graphitic carbonitride (g-C_3N_4) is a polymeric material consisting of carbon, nitrogen, and an admixture of hydrogen. It is formed by the tri-s-triazonium rings cross-linked by trigonal nitrogen atoms. It is the most stable allotrope of carbon nitrides in the presence of air. It has many surface properties which, due to the presence of basic surface sites, are attractive for many applications such as catalysis. These are e.g. basic surface features, the presence of free electrons, or H-bonding motifs. High thermal stability and hydrothermal stability (insolubility in acidic, basic, and neutral solvents), allow the material to function in both liquid and gaseous states at elevated temperatures, which is useful for heterogeneous catalysis [3,4]. The fact polymeric gCN is also responsive to visible light, has a narrow band gap (2.7 eV), is non-toxic, easy to synthesize from inexpensive precursors, and is metal-free has gained much attention in photocatalysis research [5].

The binders serve as a mechanical support for the gCN as well as a protective layer for the substrate. Currently, siloxane-based copolymers are used to improve cyclic stability. Methyltriethoxysilane has been used as a siloxane precursor and oligomeric siloxane condensate with methyl moieties was synthesized [6]. Due to the organosilica binder, we can obtain porous layers in conjunction with gCN so that successful adsorption of pollutants to the surface of the photocatalyst grains, which are deposited deeper in the layer occurs [7]. The methyl moieties provide solubility and prevent gelation but reduce the hydrophilicity of the system and limit the electron transfer and holes generated in

the gCN. To avoid these effects the siloxane binder can be mineralized (e.g., by UV or plasma) to SiO_2, completely inorganic silica [6].

Thus, using graphitic carbonitride and a proprietary oligomeric siloxane binder, we can create formulations that, when deposited on substrates, form photocatalytic layers with great potential for future applications. In this work, we focus on mechanochemical modifications of gCN and optimize the binder-catalyst ratio by investigating the reactivity between gCN and the siloxane binder.

2 Experimental

2.1 Synthesis and milling of graphitic carbonitride

Melamine and cyanuric acid were used to synthesize the supramolecular gCN complex [8]. Their solutions were left on the shaker for 20 min at 250 rpm and then mixed in a 1:1 ratio and later stirred for another four hours. The obtained mixture was subjected to centrifugation at 3000 rpm for 10 min. The sediment after centrifugation was dried overnight in an oven heated to 90°C, after reaching a constant weight. The dried complex was calcined in a covered aluminum crucible in an oven heated to 550°C under a nitrogen atmosphere. After the calcination process, the final product, crude graphitic carbonitride, was collected.

The crude product was subjected to wet milling using glass beads in isobutanol. This ensured a uniform particle size and distribution suitable for coating. The proposed wet ball milling equipment with stainless steel mixing blades was used for milling. The device was filled with 6 g of crude gCN dispersed in 54 g of isobutanol together with 45 g of glass milling balls of 1 mm diameter. The device was operated at 850 rpm for 72 hours. After completion of grinding, the beads were separated using a nylon mesh from the ground extract which had a 10% yield by weight. Thus, a stock dispersion of gCN was obtained for further formulations.

2.2 Synthesis of binder and mixing formulations with gCN

A proprietary siloxane binder with methyl functional groups was formed from trietoxymethylsilane and a solution of HCl in water. The trietoxymethylsilane solution was placed on a magnetic stirrer and drops of HCl solution were added to the volume at pH 1. The resulting solution was covered and left on the magnetic stirrer for at least 20 minutes with constant stirring. The solution was diluted to a final concentration of 20% after its formation and left in the freezer. For formulation with gCN, the resulting siloxane binder was further diluted to a concentration of 10%.

The coating formulations were prepared by mixing different weight ratios of gCN stock solution and binder solution (see Table 1).

Table 1: Formulations of compositions

Sample code	Percentage composition by weight	
	% GCN	% siloxane
A	99	1
B	98	2
C	96	4
D	92	8
E	84	16
F	68	32

2.3 Coatings and modification

The resulting formulations were deposited on soda-lime glass slides and FTO substrates using a Mayer rod (spiral rod). The deposition method ensured uniformity in the thickness of the wet films, namely 30 microns. After deposition, the films were dried at 120°C for 1 h and further stored at ambient temperature in dust-tight containers. To avoid problems made by methyl groups, the siloxane binder had to be mineralized to amorphous silica, thereby increasing the activity of the surfaces. The mineralization took place in a glass container where slides were placed and the bottom covered with about 1 cm of water to prevent overheating under a high-pressure mercury lamp, which provides radiation in the UV-A and UV-B ranges. The total UV-curing radiant exposure was 80 J/cm^2.

2.4 Methods of measurement

After curing, the physicochemical properties of the substrates were investigated. XRD was measured on an Empyrean instrument using HighScore Plus software. SEM was recorded by a Vega Tescan 2 LSH scanning electron microscope. Layer height and mechanical properties were investigated with a Dektak XT mechanical profilometer. Infrared spectroscopy was measured by a Nicolet iS50 ATR-FTIR spectrometer. Photocatalyst activity was investigated using a photocatalytically reduced resazurin probe. An Ocean Optics Maya compact spectrometer with a fiber optic sampling attachment and OceanView software was used.

3 Results and Discussion

3.1 Effect of milling and binder on gCN particles

XRD method was used to investigate the effect of milling where samples of raw powder without milling, milled stock slurry, and formulations A and F were measured. The formulations that differed most in binder content were selected to investigate their effect on the ground particles. A diffractogram can be seen in Fig. 1, demonstrating that the unground particles have greater diffraction than the ground form of the catalyst. However, the grinding preserves the particle structure, demonstrating only a small peak broadening at the stock suspension. Formulations A and F show the same signal, which is due to their same particle source but with lower intensity relative to the binder-free samples. Its influence can be observed in the range 2θ=8~16° where the presence of an amorphous phase of siloxane condensate is visible in formulation F, which contains the highest amount of the binder.

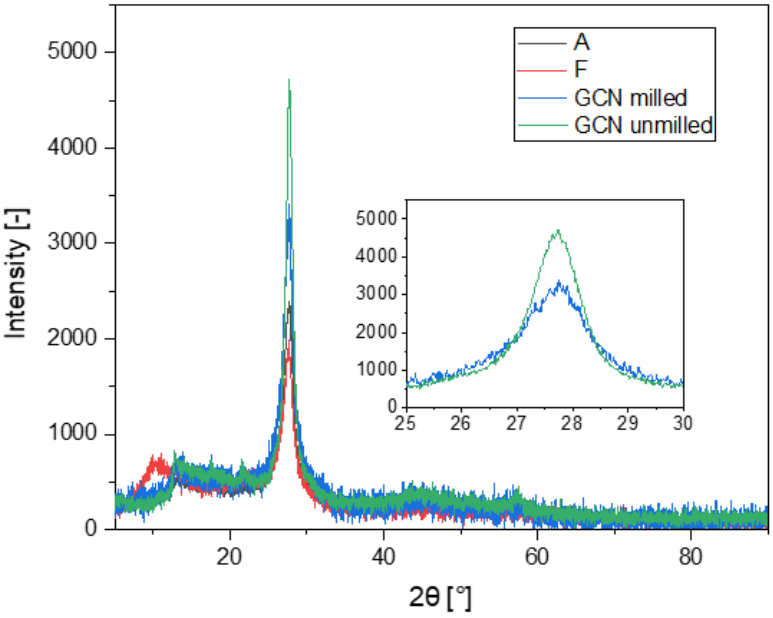

Figure 1: Diffractogram of gCN particles

3.2 Effect of binder mineralization on photocatalyst layers

To use the photocatalyst layers for photocatalysis in an aqueous solution, it is necessary to convert the hydrophobic surface into a hydrophilic one. To do this, the siloxane binder must be at least partially mineralized to amorphous silica, which, unlike methyl groups, does not prevent adsorption to the catalyst surface. The effect of the mineralization of the organic groups in the siloxane binder can be observed through the FTIR images in Fig. 2. The observed substrate sample contained formulation F with the highest binder content in both the untreated form and the sample after UV curing. In Fig. 2, the peak decrease at 2950 cm^{-1}, corresponding to the C-H vibration, can be seen. This change also contributed to the changes in the physical properties of the coating by changing to a hydrophilic nature of the coating suitable for catalysis in aqueous solutions.

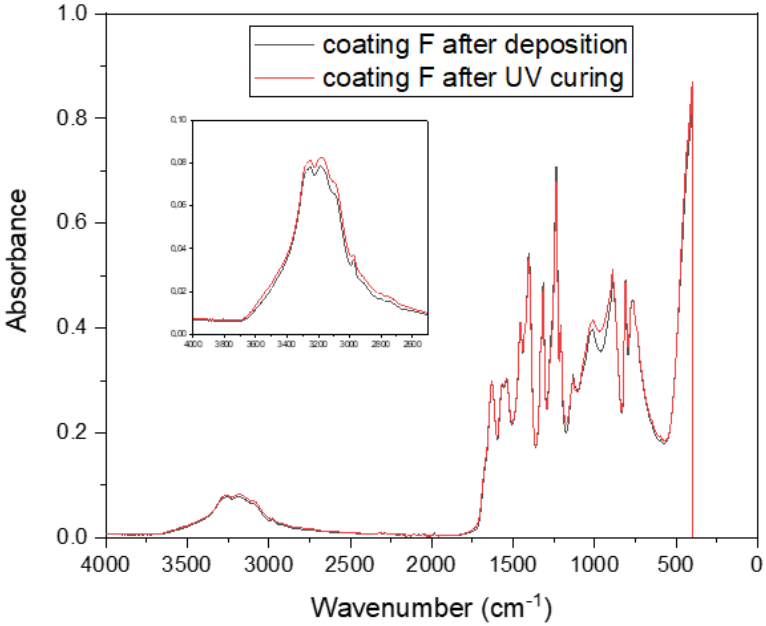

Figure 2: FTIR measurement results for F-type coating

3.3 Determination of photocatalyst activity

The fluorescent dye resazurin was used as a model contaminant to determine the photocatalytic activity of our coatings. Resazurin undergoes photocatalytic reduction to the highly fluorescent resorufin at λ_{max} =590 nm. The initial rate of conversion of resazurin to resorufin (rate of fluorescence change) was monitored and thus the photocatalytic activity of the sample was defined. More active samples produce a steeper initial rate. Fig. 3 shows the average results from several measurements demonstrating the activity of the different gCN and binder formulations on the substrates.

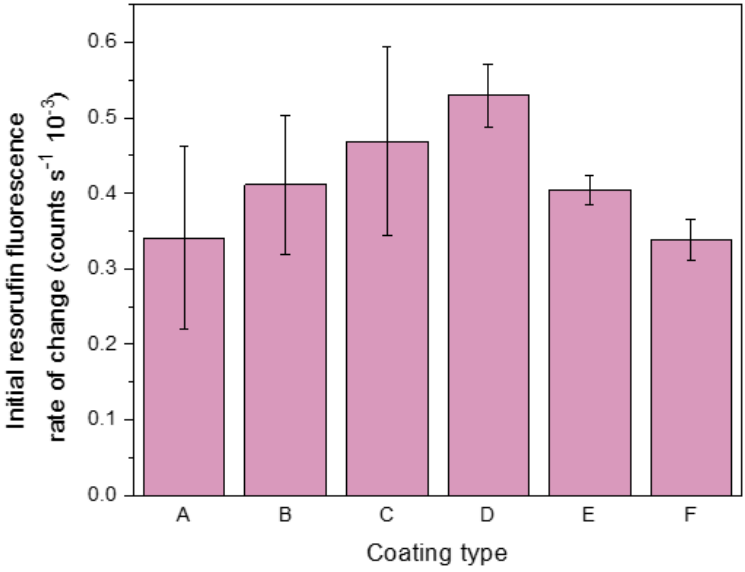

Figure 3: Expression of the photocatalytic activity of a series of samples

This experiment also demonstrated that some formulations are susceptible to damage. Coatings A and B were very susceptible to surface wear and the disruption of the coatings was present. Sample C, although not disturbed in the reaction, was still susceptible to mechanical damage. The other formulations D-F were not susceptible to damage and adhered to their substrates during measurements.

3.4 Surface properties of applied coatings

After the coatings were applied to the substrates and cured, it was not possible to observe much visual change with the naked eye between formulations. The only visual difference was that the samples with high gCN content (A-B) were more opaque compared to those containing more binder (E-F). SEM imaging revealed several differences between the samples (Fig. 4). Sample A (left) has a more porous texture and a fluffier surface compared to sample F (left). The latter, mainly due to the high binder content, has a more compact surface and the particles appear less aggregated compared to the surface with higher gCN content.

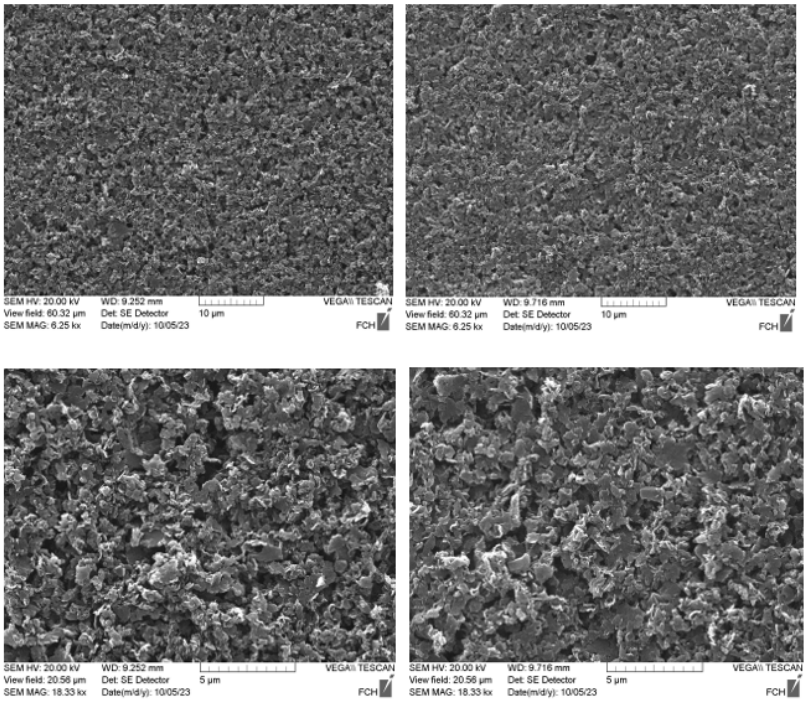

Figure 4: SEM view of selected samples

Due to the siloxane binder content, the individual coatings differ in height and resistance to damage, which was measured using a mechanical profilometer. The surface of each formulation was scratched, allowing a profilometric scan, producing a record of the height of each coating (Fig. 5). The height of the coatings decreased as the binder content increased, which could have been caused by evaporating the organic solvent from the surfaces during the drying and curing process. This measurement confirms the results measured by SEM-the layers with higher binder content are more compact.

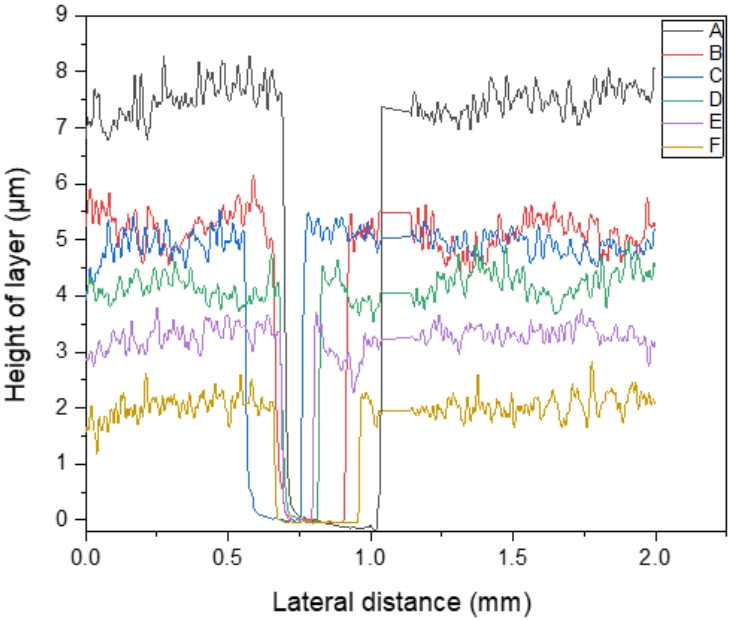

Figure 5: Profilometric record of coating height

In the next step, it was necessary to include the hardness of the layers and therefore their scratch resistance in the measurements. Also, the measurement of the layer hardness was investigated thanks to a mechanical profilometer. In this measurement, the tip pressure was varied and the force that the tip had to exert to cause mechanical damage to the layer was recorded. The results of this test can be seen in Table 2, where the pressures from each measurement are averaged. From the results, it can be seen that in the hardness test, the scratch resistance increased with increasing binder content.

Table 2: Results of micro scratch testing

Sample code	Critical tip force of 3 independent traces (mg)			Mean critical force (mg), i.e. layer hardness
A	8.0	7.0	7.5	7.5
B	7.5	8.0	7.0	7.5
C	8.0	8.5	8.0	8.2
D	14.5	14.5	14.5	14.5
E	15.0	15.0	14.5	14.8
F	>15	>15	>15	>15

Because of the measured results, it is clear that the formulation with the best properties will have to arise from trade-offs between mechanical resistance, layer height/porosity as well as the photocatalytic activity of the individual coatings.

4 Conclusion

From the obtained results, we can conclude the appropriate manipulation of gCN, the binder, and obtaining their appropriate ratio for further use. During sample preparation, wet milling proved to be very effective in controlling the particle size which retains its crystallinity. The proprietary siloxane binder used in the formulation of the gCN formulations proved to be suitable for ensuring surface compactness on the substrates. Thanks to FTIR spectrometry, we also concluded that after UV curing, mineralization occurs, making the coating suitable for photocatalytic purposes in aqueous environments. In general, the higher the gCN content the better the photocatalytic properties of the surfaces should be. This trend is also supported by the results from the mechanical profilometer, which recorded higher layer height values for coatings with higher photocatalyst content, indicating greater porosity of the coatings. However, the formulations with lower binder content deteriorated with repeated use and hardness tests showed that they were indeed more susceptible to deterioration due to their non-compactness. This also made samples A, B, C more susceptible to errors in the measurement of their photocatalytic activity as they were easily worn away by repeated measurements. The best compromise between the mechanical and surface properties of the coatings versus their photocatalytic activity is formulation D. Formulation D contains 92 wt% gCN and 8 wt% binder. Its photocatalytic properties make it the formulation with the best properties among the formulations with high photocatalyst content, and the durability of the coating is comparable to formulations with higher binder content.

5 Acknowledgment

This work received financial support from the Grant Agency of the Czech Republic through the project 23-06843S.

6 References

1. CHEN, Mengmeng, Mengxue LI, Stephanie Ling, Jie LEE, Xi ZHAO and Sijie LIN. Constructing novel graphitic carbon nitride-based nanocomposites - From the perspective of material dimensions and interfacial characteristics. Chemosphere (Oxford) [online]. England: Elsevier, 2022, 302, 134889-134889 [cited 2023-01-26]. ISSN 0045-6535. Available from: doi:10.1016/j.chemosphere.2022.134889
2. REDDY, Kakarla Raghava, CH. Venkata REDDY, Mallikarjuna N. NADAGOUDA, Nagaraj P. SHETTI, Shim JAESOOL, and Tejraj M. AMINABHAVI. Polymeric graphitic carbon nitride (g-C3N4)-based semiconducting nanostructured materials: Synthesis methods, properties and photocatalytic applications. Journal of environmental management [online]. England: Elsevier, 2019, 238, 25-40 [cited 2023-01-28]. ISSN 0301- 4797. Available from: doi:10.1016/j.jenvman.2019.02.075
3. ZHU, Junjiang, Ping XIAO, Hailong LI and Sonia A. C CARABINEIRO. Graphitic Carbon Nitride: Synthesis, Properties, and Applications in Catalysis. ACS applied materials & interfaces [online]. WASHINGTON: American Chemical Society, 2014, 6(19), 16449- 16465 [cited 2023-01-30]. ISSN 1944-8244. Available from: doi:10.1021/am502925j
4. DONG, Guoping, Yuanhao ZHANG, Qiwen PAN and Jianrong QIU. A fantastic graphitic carbon nitride (g-C3N4) material: Electronic structure, photocatalytic and photoelectronic properties. Journal of photochemistry and photobiology. C, Photochemistry reviews [online]. Elsevier B.V, 2014, 20, 33-50 [cited 2023-01-31]. ISSN 1389-5567. Available from: doi:10.1016/j.jphotochemrev.2014.04.002
5. DARKWAH, Williams Kweku and Yanhui AO. Mini Review on the Structure and Properties (Photocatalysis), and Preparation Techniques of Graphitic Carbon Nitride Nano-Based Particle, and Its Applications. Nanoscale research letters [online]. New York: Springer US, 2018, 13(1), 388-15 [cited 2023-01-31]. ISSN 1931-7573. Available from: doi:10.1186/s11671-018-2702-3
6. SVOBODA, Tomáš, Michal VESELÝ, Radim BARTOŠ, Tomáš HOMOLA and Petr DZIK. Low-temperature mineralisation of titania-siloxane composite layers. Catalysts [online]. Basel: MDPI, 2021, 11(1), 1-13 [cited 2023-05-02]. ISSN 2073-4344. Available from: doi:10.3390/catal11010050
7. GRÉGORI, D., I. BENCHENAA, F. CHAPUT, S. THÉRIAS, J.-L. GARDETTE, D. LÉONARD, C. GUILLARD and S. PAROLA. Mechanically stable and photocatalytically active TiO 2 /SiO 2 hybrid films on flexible organic substrates. Journal of materials chemistry. A, Materials for energy and sustainability [online]. 2014, 2(47), 20096-20104 [cited 2023-05-02]. ISSN 2050-7488. Available from: doi:10.1039/C4TA03826F
8. S. Dolai, SK Bhunia, P. Kluson, P. Stavarek, A. Pittermannova, Solvent-Assisted Synthesis of Supramolecular-Assembled Graphitic Carbon Nitride for Visible Light Induced Hydrogen Evolution - A Review, Chemcatchem, 14 (2022).

BASIC ANALYSIS OF CONCENTRATE FROM MEMBRANE PROCESSES ON THE SITE OF AN INDUSTRIAL LAUNDRY

Jan Vespalec
Martina Repková

Brno Univerzity of Technology,
Faculty of Chemistry,
Institute of Chemistry and Technology of Environmental Protection
Purkyňova 464/118, 612 00 Brno, Czech Republic
Jan.Vespalec@vut.cz

1 Introduction

We are in a consumerist world where industrial enterprises are among the foundations of a functional economy. Most industrial enterprises need water as a heat exchange medium, wash water, and more. These enterprises must subsequently manage industrial wastewater. This industrial wastewater can be discharged into the sewerage system if it meets the sewerage regulations designed according to the applicable laws, or the wastewater can be treated and reused. In the case of industrial enterprises, the water usually needs to be treated on-site at the industrial enterprise to a water quality that meets the limits for discharge to the sewer before it can be discharged to the sewer.

"The world is moving towards a circular economy, including in the pursuit of water"[1, 2]. Thanks to the circular economy model, there are savings in thermal energy consumption and the volume of water consumed. With wastewater production, we cannot reuse industrial wastewater 100 %. Many water treatment processes can be used for water reuse, and in this work, the focus is on membrane processes.

We obtain a purified permeate and a highly concentrated concentrate in reusing industrial wastewater using membrane processes. The question is whether the concentrate from membrane processes will comply with the sewage code and whether it can be classified as hazardous waste. From the literature search in the theoretical part, we have two hypotheses: H1: "The concentrate from membrane processes meets the sewerage code", and H2: "The concentrate from membrane processes is not a hazardous waste".

2 Experimental

2.1 Monitored indicators and analytical methods

The indicators monitored were selected according to hazardous waste legislation and the limits of the sewerage regulation. A total of 10 indicators are observed: pH, Conductivity, Non-dissolved substances, Dissolved substances, Dissolved inorganic salts, COD_{Cr}, BOD_5, Nitrites, Nitrates and Ammonium cations.

2.1.1 Determination of basic physicochemical parameters

Determination of pH and conductivity was carried out on-site using a mobile pH meter and a conductivity meter (ECTestr 11+). The instrument was submerged so the probe was below the surface and waited until the value stabilised. Upon arrival at the laboratory, the pH and conductivity were measured with a more accurate HI 5522 benchtop multimeter.

2.1.2 Determination of chemical and biological oxygen demand

Determination of chemical oxygen demand using dichromate (COD) was carried out according to ISO 15705 Water quality – Determination of chemical oxygen demand (COD) - tube method[3]. Determination of biological oxygen demand was also performed, namely 7-day (BOD_7), which was subsequently converted to 5-day (BOD_5) according to EN ISO 5815-1 Water quality - Determination of biochemical oxygen demand after n days (BODn) - Part 1: Dilution and inoculation method with addition of allylthiourea[4].

Determination of COD_{Cr}

COD_{Cr} was determined using the Spectroquant® kit on a NOVA 60 spectrophotometer from Merck Ltd. Due to the large number of samples, a customised cuvette kit for COD determination was also prepared according to the bachelor thesis of Ing. Martina Švábová[5]. All working procedures were carried out according to the prescribed instructions.

Determination of BOD_5

BOD was always measured in three repetitions of the selected dilution. At least two ranges of BOD determination (two different dilutions) were always chosen according to the measured COD_{Cr} result. BOD was measured over seven days to ensure that the end of the measurement was on a working day. However, the BOD was subsequently converted to 5-day. According to Winkler, A control sample was always prepared for each determination to ensure the correct procedure was followed. BOD was evaluated based on the decrease in dissolved oxygen in the oxygen cylinder. Dissolved oxygen was measured using a Greisinger GMH 3651 portable oximeter.

2.1.3 Determination of suspended solids

Determination of suspended solids (SS) was done according to EN ISO 872 Water quality - Determination of suspended solids - Glass fibre filter method[6]. Each sample (100 ml) was measured three times from different sample tubes. One blank was also measured at each measurement, where the sample was replaced with 150 ml of distilled water. GF/CTM glass microfiber filters were used for filtration.

2.1.4 Determination of dissolved substances

Determination of dissolved substances (DS) was done according to the standard CSN 75 7346 Water quality - Determination of dissolved substances[7]. Each sample (100 ml) was measured three times from different sample tubes. One blank was also measured at each measurement, where the sample was replaced by 150 ml of distilled water. GF/CTM glass microfiber filters were used for filtration, and then the sample was dried in an oven at 105 °C in an evaporating dish.

2.1.5 Determination of dissolved inorganic salts

Dissolved inorganic salts (DIS) were determined according to the standard CSN 75 7347 Water quality - Determination of dissolved inorganic salts (DIS) in wastewater - Gravimetric method after filtration with a glass fibre filter[8]. Before each measurement, the evaporation pans were cleaned and annealed in a muffle furnace at 550 °C for one hour. Each sample (100 mL) was measured three times from different sample trays. One blank was also measured at each measurement, where the sample was replaced with 150 ml of distilled water. GF/CTM glass microfiber filters were used for filtration, and the sample was then oven-dried at 105 °C and then annealed in a muffle furnace at 550 °C in an evaporation pan.

2.2 Sampling plan

Before the actual sampling, a sampling plan was developed, which includes:

- Sampling period
  - 28.4.2022-18.1.2023
- Type of sampling
  - Active Sampling - Simple Sample
- Location and number of sampling events
  - One sampling point (plastic RO concentrate outlet) and 12 sampling events
- Specification of sampling points
  - New clean 1 litre HDPE samplers
- Sample preparation method
  - Filtration with 0.6 micron membrane filter
- Storage and preservation of samples
  - Sample storage in a refrigerator at four °C
  - Preservation of part of the sample for elemental analysis using 1 ml of concentrated HNO_3 per 100 ml of sample

2.3 Semi-operational membrane unit

A pilot semi-operational membrane unit configured and built by ASIO TECH spol. s r.o. was used in this work. The semi-operational membrane unit comprises ultrafiltration, granular activated carbon, UV lamp and reverse osmosis. Here, the UV lamp serves the role of sterilising the spray on RO to protect the membrane from biofouling, i.e. biofilm formation on the membranes.

The pilot semi-operational unit used at the industrial laundry site is shown schematically in Figure 1. The input water flowed through the heat exchanger to the

storage tank (0.5 m³). The laundry has a heat exchanger used to recover heat from the wastewater, but it is also a necessary pre-treatment for the pilot semi-operational unit technology used. This is necessary for the following reasons: increase of the solubility of the excitation during the flotation process, increase of the permeability and limitation of the thermal stability of the membrane material. Water was pumped from the storage tank to the flotation tank (2 m³), where the flotation was carried out using a recirculation pump. An ultrafiltration membrane, granular activated carbon and a UV lamp followed this. Subsequently, an antiscalant was dosed for reverse osmosis operation, which was the last stage of purification.

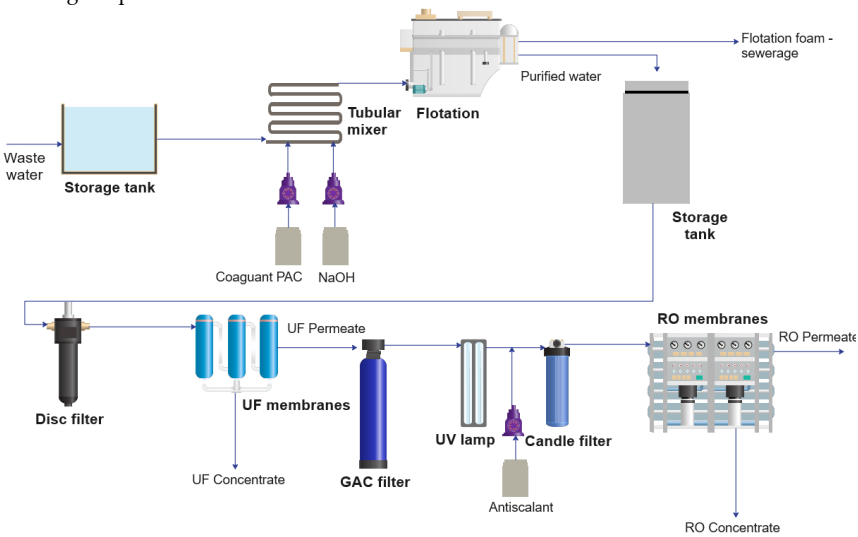

Figure 1: Schematic of a pilot semi-operational unit located in an industrial laundry

3 Results and Discussion

The measured data were evaluated in the statistical program RStudio. First, the measured data were found to be normal using the Shapiro-Wilk, Anderson-Darling and Shapiro Francia tests. For Gaussian distribution data, both parametric estimates of position and variability (mean and standard deviation) and non-parametric estimates of position and variability (median and median absolute deviation) were performed. In addition, confidence intervals for each estimate were calculated. For data identified by normality tests for non-Gaussian distributions, the trimmed mean and standard deviation were calculated, the nonparametric estimates of position and variability (median and median absolute deviation) were calculated, and the confidence interval for each estimate was calculated. Each indicator was tested by one-sided t-test against the cut-off values in the case of a Gaussian distribution, and the Wilcoxon test was used in the case of a non-Gaussian distribution.

In the results table, an asterisk symbol is shown for samples that are not Gaussian distribution according to the normality test result. For these samples, statistics were performed using non-parametric methods.

The statistically evaluated data are plotted in a boxplot with the following sampling point labels: input data (VS), UF permeate data (UFP), RO concentrate data (ROK), and RO permeate data (ROP). The thick line in the boxplot indicates the median. The boxplot is the interquartile range (IQR) between the 1st and 3rd quartiles. The line from the boxplot indicates the range of values within 1.5 times the IQR. The actual detection limit in a particular boxplot is plotted for samples below the detection limits.

The samples are compared to the Sewage Regulations (SR) limits at the industrial laundry sampling location. Also, the samples are compared to the hazardous waste (HW) classification limits to determine if the concentrate should be managed as hazardous waste.

3.1 Basic physicochemical parameters

The basic physicochemical parameters are pH and conductivity. According to the results of statistical tests for normality, the pH from the RO concentrate and conductivity from the RO inlet and permeate are not Gaussian distributed.

Table 1 shows the pH indicator, which is within the range of the hazardous waste and sewer regulation limits. The confidence intervals are also within these ranges. The conductivity results show a pattern of solute removal. There was an increase in conductivity when comparing the UF permeate and inlet due to using a higher amount of coagulant. The reverse osmosis process significantly affected the decrease in conductivity, where concentrating in the concentrate occurred.

Table 1: Statistically evaluated values of basic physicochemical parameters in the format: median ± median absolute deviation (median confidence interval)

Indicator (limit)	**Entry**	**UF-permeate**	**RO-concentrate**	**RO-permeát**
pH [–] (SR: 6,5–9,5; HW: 5,5–13)	9,95 ± 0,18 (9,71–9,86)	7,8 ± 0,4 (7,0–7,7)	* 7,8 ± 0,2 (7,4–7,8)	8,1 ± 0,4 (7,7–8,0)
Conductivity [μS·cm^{-1}]	* 1 269 ± 117 (1 171–1 212)	1 581 ± 207 (1 373–1 570)	3 806 ± 1 116 (3 392–3 682)	* 26 ± 3 (19–25)

3.2 Chemical and Biological Oxygen Demand

The chemical and biological oxygen demand indicators were predicted to be elevated at the industrial laundry site due to the use of tensides in laundry operations. Statistical analysis showed that all measured data were Gaussian in distribution.

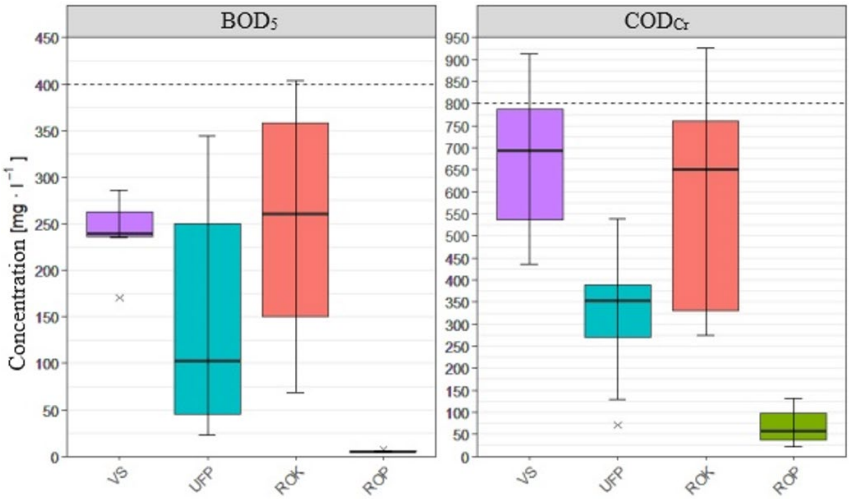

Figure 2: Statistically evaluated chemical and biological oxygen demand values

The COD_{Cr} and BOD_5 indicators are not evaluated in the hazardous waste framework HP 15. However, the indicators are controlled within the sewerage regulation. BOD5 is limited in sewerage regulations to a value of 400 mg·l^{-1}. This value is indicated in the graph in Figure 2. This limit value is close to the confidence interval value of the mean. Even in the graph in Figure 2, the limit is exceeded by values of 1.5 times the IQR. Thus, the BOD_5 indicator is close to the limit value and cannot be conclusively determined whether it meets the limit. The COD_{Cr} indicator has a sewer code limit of 800 mg·l^{-1}, as indicated in the graph in Figure 2. Both confidence intervals and IQRs are close to the COD_{Cr} limit. Therefore, this indicator also cannot be shown to meet the limit, as it is suspected that occasional exceedances of the limit could occur.

5.3 Suspended and dissolved substances

This section lists and discusses the results for suspended solids, dissolved solids, and dissolved inorganic salts. Statistical analysis revealed that DS from RO permeate and SS from UF permeate are not Gaussian distributed. The remaining data are Gaussian in distribution, but the normality test was not performed for the selected SS and DIS data, which took values lower than the detection limit. All SS contained in the UF permeate, RO concentrate, and RO permeate are smaller than the pore size of the ultrafiltration membrane, namely 0.02 μm.

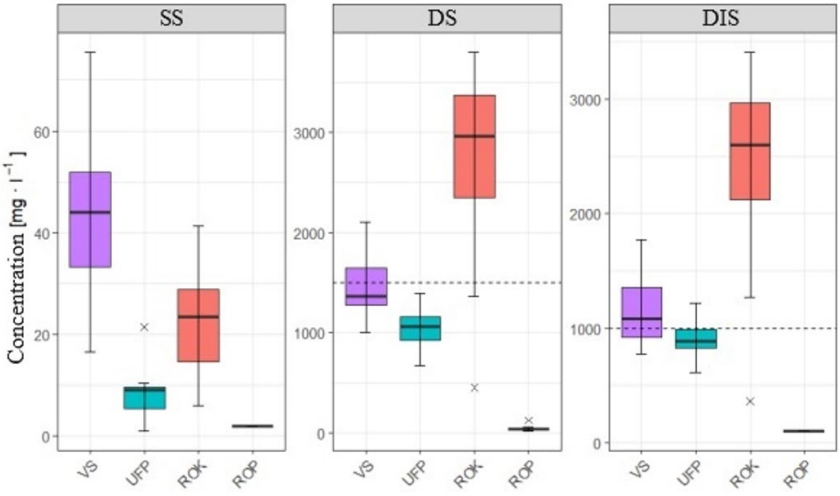

Figure 3: Statistically evaluated values of suspended and dissolved solids

Suspended solids are included in the sewer regulations limits at 350 mg l^{-1}. The measurement results are demonstrably below this limit. The graph in Figure 3 shows that most of the SS were separated on ultrafiltration. Only substances up to 0.02 μm in size passed into the UF permeate (median 8.6 mg·l^{-1}) and were subsequently separated on the RO to the concentrate, where the NL concentration tripled.

Dissolved solids are evaluated in the HP 15 hazardous waste limits and the sewer regulations. HP 15 has a limit of 8,000 mg·l^{-1} - this limit has been demonstrated to be met. However, the SR is more stringent; the limit is 1,500 mg·l^{-1}. This limit has been exceeded by approximately twice that amount. Such wastewater cannot, therefore, be discharged freely into the sewer, and the sewerage undertaker must be contacted.

Similar to DS, dissolved inorganic salts were also assessed in the SR, and the limit was also shown to be exceeded almost three times. Again, such wastewater cannot be discharged freely into the sewer, and the sewerage operator must be contacted. The difference between the DIS and DS values (approximately 350 mg·l^{-1}) shows how much of the suspended solids were of organic origin. These can be, for example, tensides, hydrocarbons, oils, personal care products and others.

Conclusion

Concentrate evaluated against three limits. The first limit is the sewerage regulations issued by the sewerage operator in the sampled location. Decree No. 8/2021 Coll defines the second limit., precisely sentence HP 15, and the indicators selected from there. The statistically processed results show that the reverse osmosis concentrate does not meet the limits of the selected indicators of the sewerage regulation, namely COD_{Cr}, BOD_5, DS and DIS. The statistically processed results also show that the reverse osmosis concentrate

meets the limits of selected indicators from the HP 15 hazardous substances sentence. The appropriate way to deal with the resulting concentrate is to first negotiate with the sewerage and wastewater treatment plant operator to increase the limit of the SR and the possibility of discharging the defined wastewater into the sewerage. Alternatively, the concentrate can be further treated, e.g. with ZLT technologies, and then treated as anhydrous waste. The last option is to ask an external specialist company to treat the wastewater. This, therefore, rejects hypothesis 1, 'Membrane process concentrate complies with the sewerage code' and confirms hypothesis 2 'Membrane process concentrate is not hazardous waste', which were defined in the introduction.

4 References

1. Cirkulární Česko – Ministerstvo životního prostředí [online]. [2023-03-03]. Available from: https://www.mzp.cz/cz/cirkularni_cesko
2. STRATEGICKÝ RÁMEC CIRKULÁRNÍ EKONOMIKY ČESKÉ REPUBLIKY 2040 [online]. 2021 [2023-03-03]. Available from: https://www.mzp.cz/C1257458002F0DC7/cz/cirkularni_cesko/$FILE/OODP©Cirkularni_Cesko_2040_web-20220201.pdf
3. ČSN ISO 15705 Jakost vod – Stanovení chemické spotřeby kyslíku (CHSKCr) - Metoda ve zkumavkách. Praha: Český normalizační institut, 2008. 24 s.
4. [79] ČSN EN ISO 5815-1 Kvalita vod – Stanovení biochemické spotřeby kyslíku po n dnech (BODn) - Část 1: Zřeďovací a očkovací metoda s přídavkem allylthiomočoviny. Praha: Český normalizační institut, 2020. 28 s.
5. ŠVÁBOVÁ, Martina. Optimalizace koagulačního postupu při čištění odpadní vody. [online]. Brno, 2019 [2023-04-07]. Bakalářská práce. Vysoké učení technické v Brně, Fakulta chemická,. Available from: https://www.vutbr.cz/studenti/zav-prace/detail/113498.
6. ČSN EN ISO 872 Jakost vod – Stanovení nerozpuštěných látek – Metoda filtrace filtrem ze skleněných vláken. Praha: Český normalizační institut, 2005. 12 s.
7. ČSN 75 7346 Jakost vod – Stanovení rozpuštěných látek. Praha: Český normalizační institut, 2002. 12 s.
8. ČSN 75 7347 Jakost vod – Stanovení rozpuštěných anorganických solí (RAS) v odpadních vodách – Gravimetrická metoda po filtraci filtrem ze skleněných vláken. Praha: Český normalizační institut, 2009. 12 s